Chapter 3. SAR Measurements of Sea Ice

Robert G. Onstott
General Dynamics - Advanced Information Systems, Ann Arbor, MI, USA

Robert A. Shuchman
Altarum (formerly ERIM), Ann Arbor, MI, USA

3.1 Introduction

This chapter presents the fundamentals of active microwave remote sensing of sea ice. It begins with a description of the various sea ice forms and characteristics, explains what type of ice information may be retrieved from Synthetic Aperture Radar (SAR) imagery and concludes by examining a number of typical SAR image examples.

Sea ice covers between 11% and 15% of the earth at the Polar Regions. In the Arctic the permanent ice cap exists above 72°N latitude and can extend as far south as the mid-latitudes during the winter. It is important to characterize sea ice because its extent and duration has an effect on the global climate and presents a hazard to shipping. Since the polar regions are dark during at least half the year and are often cloud covered, active microwave sensors including altimeters, scatterometers, real aperture radars (RARs) and synthetic aperture radar (SARs) are the most useful remote sensing instrumentation for these regions. Active microwave sensors are generally unaffected by the atmosphere, solar illumination, or precipitation. When placed on a polar orbiting satellite, these sensors provide reliable and periodic observations of sea ice extent and conditions in the Polar Regions.

Since the late 1970s, seasonal investigations in the Arctic during the fall freeze-up, late winter, spring, and summer have been conducted to acquire empirical data that describes the microwave properties of sea ice. These data, collected over a wide range of frequencies, polarizations, and angles of incidence, contribute to studies to determine the ability of microwaves to classify ice type and to characterize the physical and electrical properties that control emission and backscatter levels. By understanding the processes and properties responsible for producing microwave signatures from sea ice, it has been possible to develop approaches to retrieve critical geophysical parameters including: edge characteristics, type, floe size distribution and concentration, thickness, age, and snow cover.

Sea ice is the most complex earth terrain. This complexity is due to the many possible forms of sea ice, and to the fact that sea ice properties and physical structures are continuously modified by ocean and atmospheric dynamics. For instance, the conditions during which ice forms impact its immediate physical and electrical properties, and influence all future properties as it ages. As an example, sheets of young ice formed under quiescent conditions may be transformed into a reasonably flat, reasonably thin slab of rafted ice whose physical and radar properties are dramatically changed. Because of the array of possible ice forms, there are at least 30 terms used to identify sea ice form and condition. In contrast, seawater measurements are less complicated; one factor that helps is that there is a limited range of possible seawater dielectric constant values, whereas for sea ice the dielectric constant ranges from that of seawater to that of pure ice—an order of magnitude difference. Roughness scales for both mediums range from the almost perfectly smooth to hills of dielectric material 15 meters in height.

Additional references that detail sea ice behavior include the Geophysical Monograph 68

titled Microwave Remote Sensing of Sea Ice [*Carsey, ed.*, 1992], and the Remote Sensing of Sea Ice and Icebergs [*Haykin et al*., 1994]. A detailed discussion of SAR and scatterometer signatures of sea ice is provided in *Onstott et al.*, [1982].

3.2 Sea Ice Characteristics

Sea ice is produced when seawater freezes. This process requires that the layer of seawater at the air-sea interface has cooled to about –1.8°C (when seawater has a salinity of about 33 ppt). The form that ice takes depends upon the sea state, wind, and temperature conditions at the time of ice formation. Since there is a wide range of possible formation conditions (e.g., just below the freezing temperature vs. extreme cold, calm vs. wave agitated, low wind vs. high wind, and snowing vs. not snowing) the newly formed ice categories include a number of ice forms.

If there is no wind or waves, long ice crystals form into a very thin, very smooth layer of ice at the air-water interface (see Figure 3.1a). If wind or waves are present, then fine ice spicules become suspended in water (frazil ice) instead. As ice formation continues, the wave and wind action causes the ice crystals to coagulate and form a soupy layer (grease ice). Further accumulation results in the formation of clumps (shuga). When ice reaches a thickness greater than about 1 cm, clumps will harden into pancakes (see Figure 3.1b), and eventually into small pans (see Figure 3.1c). Newly formed ice of pancake origin has a very rough surface that is wetted with seawater. If snow falls onto the ocean surface during ice formation, slush ice will form.

Cold temperatures will cause additional freezing of sea ice at its bottom and along the sides of ice floes, thereby increasing its thickness. The rate of ice growth is highest when the ice is thinnest, and slows as ice thickens. New ice grown under quiescent conditions is described according to its visual properties that are also related directly to its thickness: nilas (black ice with thickness up to 10 cm), grey (thickness of 10 to 15 cm) and grey-white (thickness of 15 to 30 cm). After ice has reached a thickness of 30 cm, it is then known as first-year ice. While there is no upper limit on the thickness of first-year ice (see Figure 3.1d), it generally does not attain thickness greater than 2.5 m unless a deformation process is involved.

During the freezing process, a large quantity of brine is rejected from the ice back into the ocean, but some remains as impurities located at the boundaries of pure ice crystals. With age, the volume of brine reduces due to salt migration [*Smith*, 1990]. However, first-year ice remains very lossy at microwave radar frequencies even though its salinity ranges from 4 to 10 ppt limiting the distance that the radio wave penetrates into the ice medium. Furthermore, first year ice has few internal gas bubbles of a size one tenth or greater than the radar wavelength (see Figures 3.2a and 3.2b) that can produce a measurable internal volume scatter. Of the other discontinuities present in the ice (e.g., brine includes and drain tubes), they are even smaller. Hence the predominant scattering mechanism for first year ice is surface scattering.

During summer, the snow pack on sea ice melts. Free water percolates through the ice interior, flushing brine from the ice to the ocean. If first year ice survives the summer melt and reaches its second ice growing season, it will have undergone three major modifications: (a) desalination, (b) development of an undulating surface topography caused by the erosion effect of summer melt, and (c) a reduction in the density of the uppermost layer of the ice sheet.

Multiyear (MY) ice is ice that has survived more than one melt season (see Figure 3.1e). It can be distinguished from first-year (FY) ice by its greater thickness. At the end of the ice

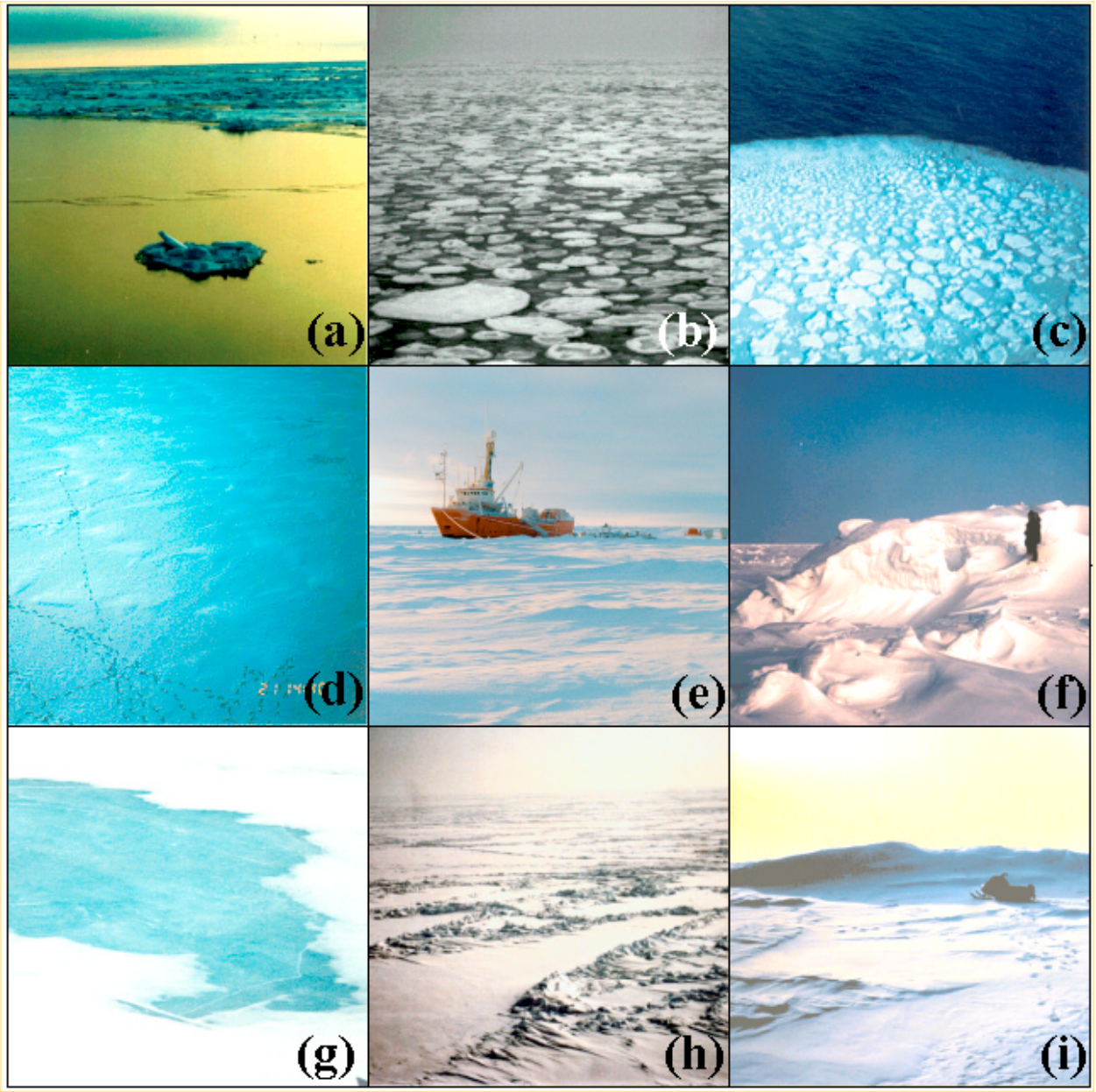

Figure 3.1. Photographs of a variety of sea ice types and forms: (a) new, (b) pancake, (c) marginal ice zone, (d) first year, (e) multiyear, (f) multiyear hummock, (g) multiyear meltpool, (h) first year pressure ridges, and (i) old multiyear pressure ridge ice.

growing season, level multiyear ice typically has a thickness greater than 2 m; level first year ice typically has a thickness less than 2.5 m. Multiyear ice has a lower salinity (less than 2.5 ppt versus more than 7.7 ppt for FY), and a thicker snow cover (greater than 0.2 m for MY versus less than 0.2 m for FY). The top 2 to 15 cm of a MY ice sheet is composed of ice that is almost pure, has very low loss, and has a significant reduction in density in the uppermost layer which takes the form of a significant population of gas bubbles whose diameters are between 1 and 3 mm (see Figure 3.2c).

A simplified cross-section of first year and multiyear sea ice is presented in Figure 3.3 and serves to illustrate major physical property differences between the two major ice types.

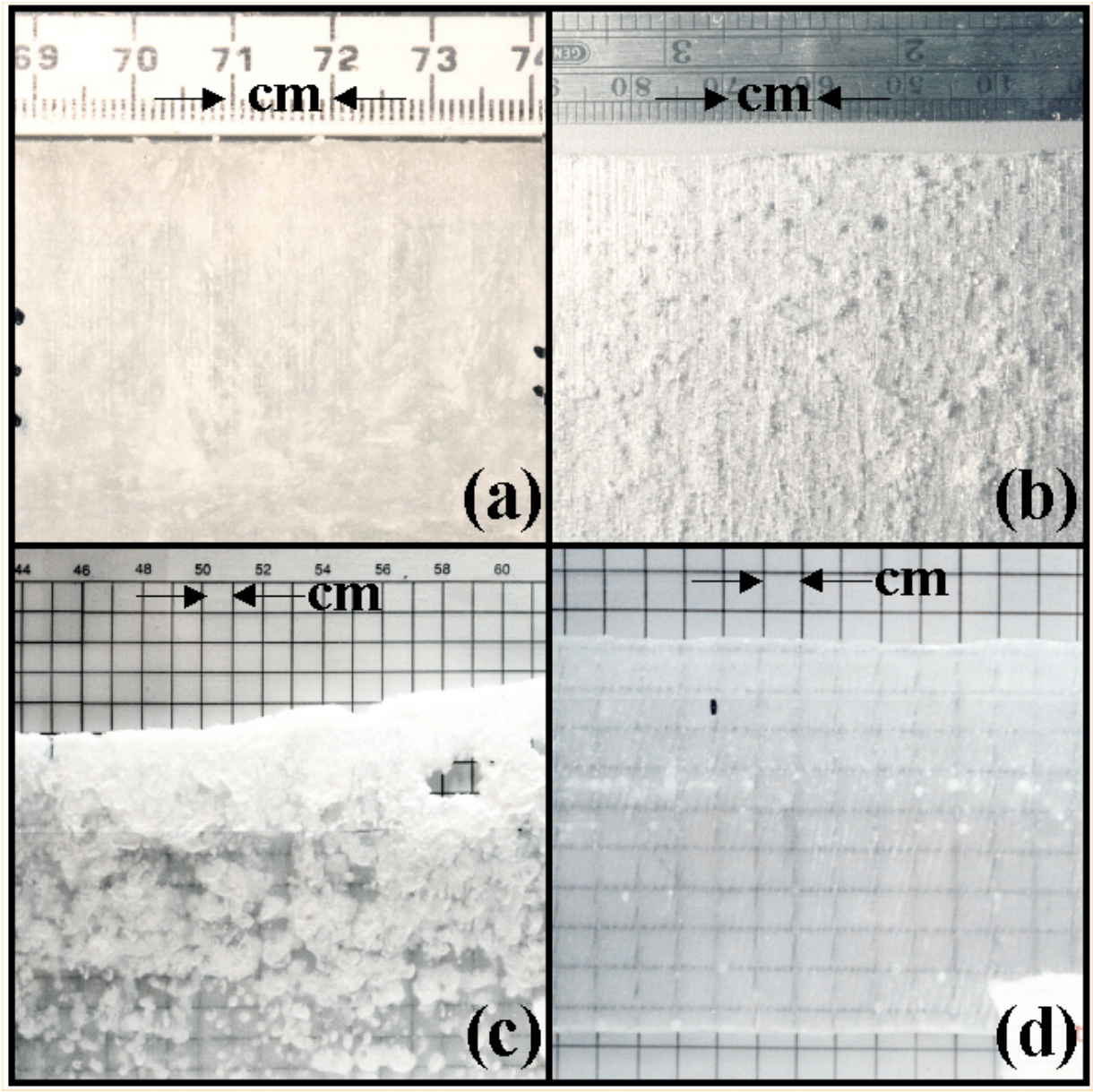

Figure 3.2. Thin sections shown with 1-cm grids for (a) new, (b) young, (c) multiyear raised, and (d) multiyear meltpool ice.

Other ice modifications of note include those associated with ice deformation (see Figures 3.1f, 3.1h, and 3.1i), and the freezing of fresh water into pools on multiyear ice (see Figure 3.1g and Figure 3.2d).

3.3 Basic Concepts of the SAR Remote Sensing of Sea Ice

Active microwave sensors including altimeters, scatterometers, real aperture radars (RARs) and synthetic aperture radar (SARs) transmit electromagnetic energy to observe targets of interest. The portion of the transmitted energy that is returned back to the radar is determined by the scattering properties of the area illuminated.

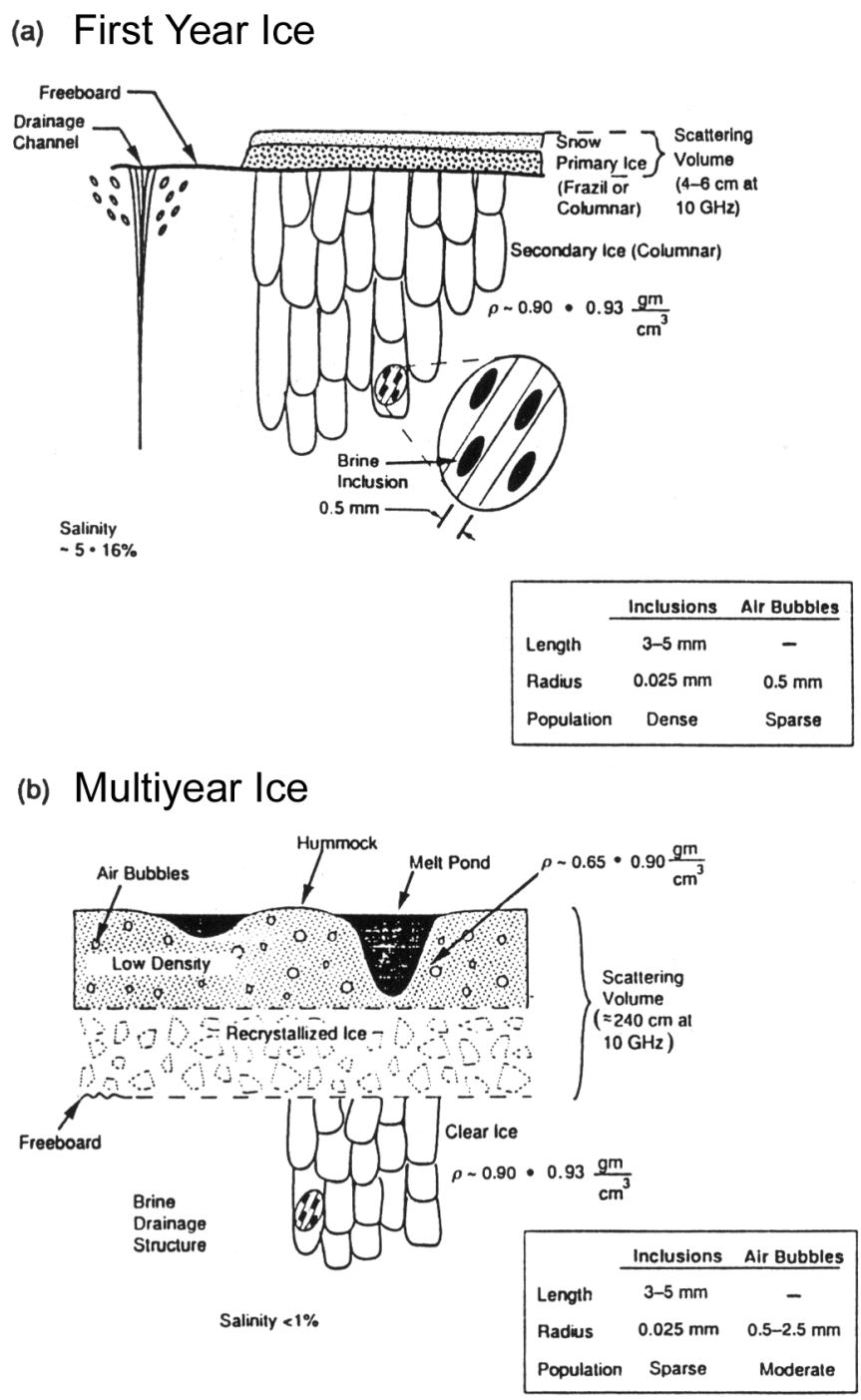

Figure 3.3. Simplified cross-section of (a) first year and (b) multiyear sea ice. [*Onstott*, 1992]

3.3.1 Backscatter Response during Winter

The radar scattering coefficient, also called the backscatter cross section, is an absolute measure of scattering behavior of the terrain under observation on a per square meter per square meter (m^2/m^2) basis. It is a function of frequency, angle of incidence, polarization, and the scattering characteristics of the illuminated area.

Combinations of four surface parameters affect the scattering characteristics of sea ice. These are:

- surface roughness (in both the small and large scales)
- dielectric constant of the sea ice (both the real and imaginary parts)
- dielectric discontinuities or discrete scatterers (such as gas bubbles in the ice)
- orientation of the ice and its surface features to the radar (azimuth look angle)

The sea state and weather conditions under which sea ice is formed has an effect on its surface roughness. The amount of surface roughness controls the distribution of the reflected energy, and thus the amount of radar backscatter. The radar return from first-year, new ice, and open water is dominated by the surface roughness.

Whether or not a surface is rough when imaged by radar is a function of the radar wavelength (l), the incident angle of the radar beam (q_i), and the average vertical displacement of the surface (Δh). Figure 3.4 shows the reflection characteristics at two radar wavelengths (X- and L-band). Lord Rayleigh developed a criterion where a surface is said to be rough if it meets the following condition:

$$\Delta h \cos q_i > \frac{l}{8} \tag{1}$$

Dielectric constant refers to the basic electrical property of all materials. It affects the amount of an incident radar wave that is reflected, absorbed, and dissipated. Ocean surfaces have a high dielectric constant with most of the radar energy being reflected at the water's surface. Penetration of radio waves into the water at microwave frequencies is negligible. The dielectric constant of sea ice is strongly dependent on the salinity of the ice. New and first year ice are very lossy due to high salinity. The distance an electromagnetic wave travels through a medium before its intensity is reduced by 1/e is referred to as the penetration depth (see Figure 3.5), and is used to gauge where, in a volume, scattering may occur. It is a function of radar frequency, incident angle, temperature, and conductivity of the ice or snow. To determine the penetration depth, the complex dielectric constant, ε*, must be known. The complex dielectric constant is defined by $\varepsilon^* = \varepsilon_o(e_r' - je_r'')$ where ε_o is the free-space dielectric constant, e_r' the relative dielectric constant, and e_r'' the relative imaginary dielectric constant. The value of ε* is dependent upon the density of the ice, the volume of the brine, and the dielectric properties of the ice and brine. The penetration depth d and loss L are determined by the following:

$$d = \frac{1}{2}\left(\frac{2pm_r e_r'}{2l_o}\left\{\left[1+\left(\frac{e_r''}{e_r'}\right)^2\right]^{.5} - 1\right\}^{.5}\right)^{-1} \tag{2}$$

and

$$L = 10\log(e^{\frac{1}{d}}) \text{ (dB/m)} \tag{3}$$

where l_o, is the wavelength for free space. At microwave frequencies, the relative permeability m_r (proportionality constant that exists between magnetic induction and magnetic field intensity) is approximately equal to 1. Longer wavelengths penetrate to a greater extent. Non-frozen water significantly reduces penetration; thus, snow cover during melt will act as an opaque filter to the

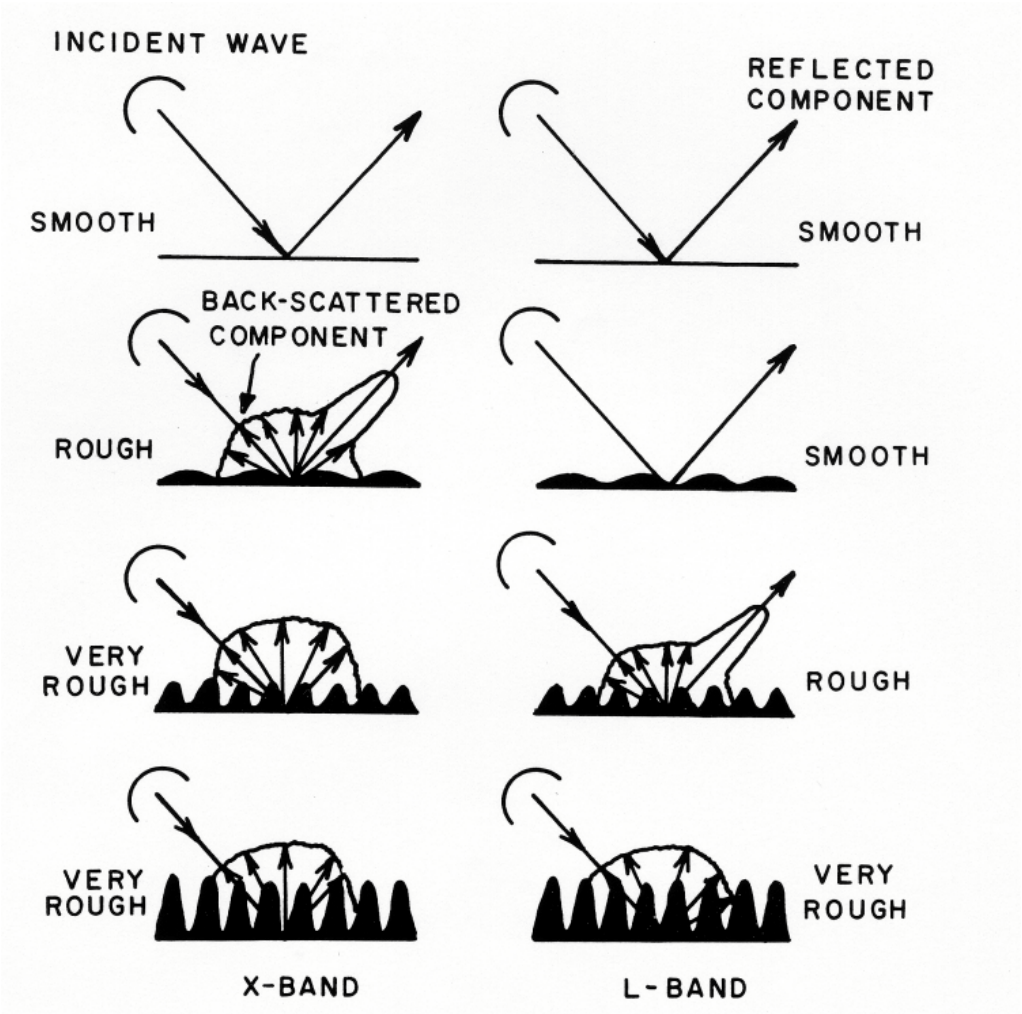

Figure 3.4. Scattering behavior of L- and X-band electromagnetic radiation for smooth, rough, and very rough surfaces.

radar waves, preventing sensing of the ice surface. Conversely, in the winter the frozen snow is transparent, allowing for imaging of the ice surface and volume. Measurements by *Vant, et al.*, [1974, 1978] indicate that first-year ice with a salinity of 7 to 8 parts per thousand at a temperature of -5°C has a penetration depth of 2 to 4 cm and a loss of about 150 dB/m at X-band (a wavelength of 3 cm). The colder the upper ice layer, the greater the penetration depth is. Multiyear ice has significantly greater penetration depth than first year ice due to a near zero salinity.

As penetration depth increases, the greater is the possible number of dielectric discontinuities or discrete scatterers in the ice (such as gas bubbles) which contribute to the radar backscatter. Multiyear ice with its lower salinity allows for microwave penetration into the ice and backscatter is dominated by volume scattering at C-band radar frequencies and higher. The bubbles and voids in multiyear ice have dimensions that are within an order of magnitude in size of the radar wavelengths at X- and C-band frequencies (e.g., 3 to 6 cm). Hence, these discrete scatterers contribute significantly to the large backscatter cross-section of multiyear ice.

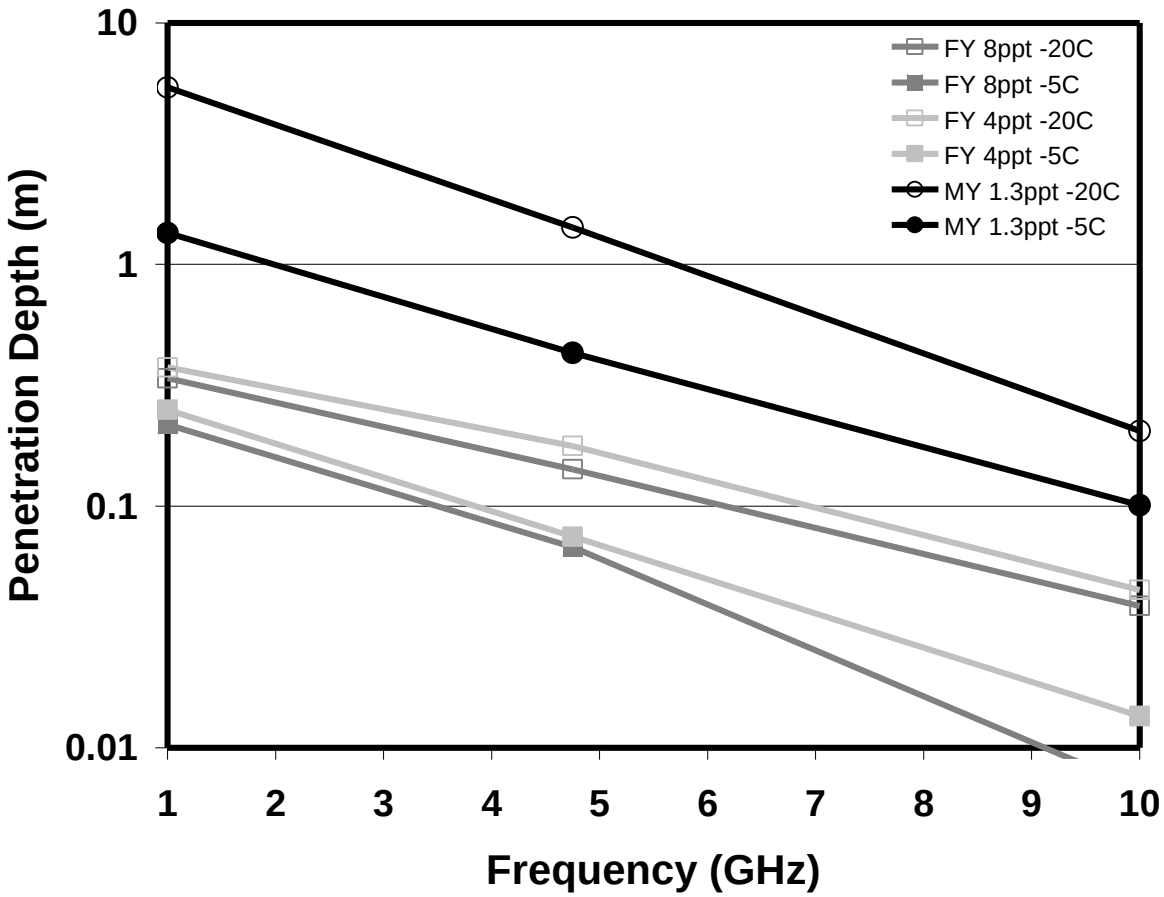

Figure 3.5. Penetration depth is shown as a function of frequency, temperature (in °C), and salinity (in parts per thousand) for multiyear ice (MY) and first year ice (FY).

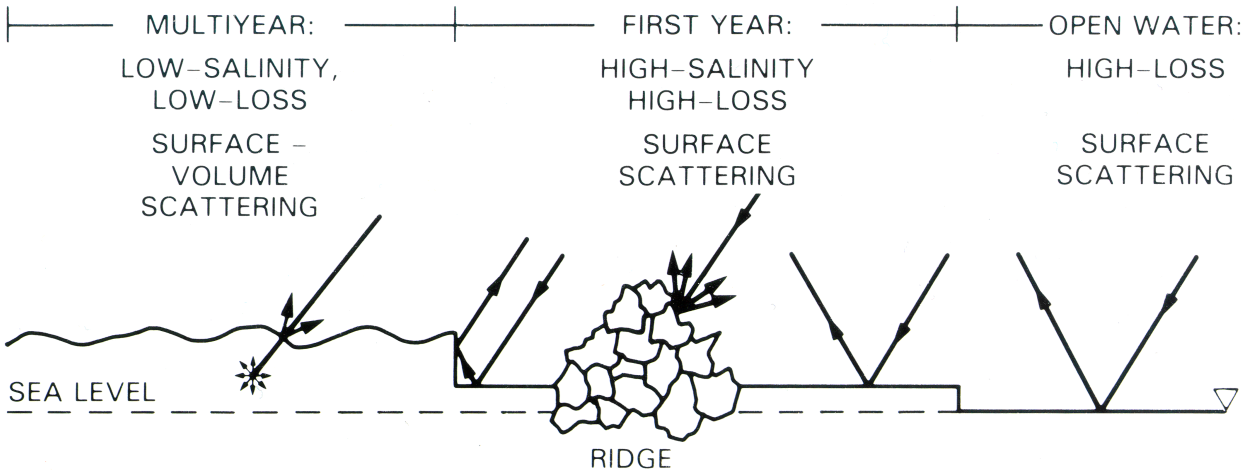

Figure 3.6. Backscatter interactions for multiyear ice, first year ice, and smooth open water. [*Onstott*, 1992]

The orientation of the ice surface features to the radar (azimuth look angle) also has an impact for cases of large-scale surface roughness (such as ice blocks strewn about the ice surface and pressure ridges). When sea ice ridges are oriented orthogonally to the radar wave propagation direction, a strong dihedral backscatter return is produced because of the reflection off of the smooth ice surfaces into the rough pressure ridge. If the radar views parallel to the pressure ridge, the number of dihedral returns are limited to the blocks within the pressure ridge , resulting in a weaker ridge response.

Figure 3.6 is a schematic of the microwave returns from water, first year ice and multiyear ice. The multiyear return is a function of surface and volume scattering since the low salinity allows penetration into the ice sheets whereas snow-free, first-year ice and ocean backscatter are dominated by scattering from the surface.

Figures 3.7 and 3.8 show measured radar backscatter cross-section data and help to illustrate the variation in radar backscatter cross sections with ice type and water signature as a function of the radar parameters of frequency (L-, C-, X-, and Ku-band), incident angle, and polarization.

3.3.2 Backscatter Response during Summer

Differentiating between ice types during summer is a complex task. Microwave signatures respond quickly to the meteorologically induced melt and freeze cycles of snow and ice surfaces, and to the formation of melt pools and the desalination of the ice sheets. During early summer, the snow pack is at its maximum annual thickness. Moist or wet snow tends to limit the backscatter response to the snow layer, and reduces any contribution from the underlying ice layer. Hence, moist snow produces backscatter signatures for thin and thick ice that are very similar, if not identical. By midsummer, the snow layer on thin and thick ice has become very thin or no longer exists and the ice surface is eroding due to melt. The signature of thin and medium first-year ice is enhanced because of a very thin or non-existent snow layer and an enhanced surface roughness associated with the ice surface. Snow on multiyear ice is often thick enough at peak melt to still produce a moist snow signature at high frequencies (such as C- and X-band), but may have enough subsurface pooling of freshwater to produce a weaker signature at L-band. In summary, at midsummer, the distribution of melt water contributes to the dynamic signatures of first year ice and a contrast reversal between first-year and multiyear ice, the two major summer ice types [*Onstott, et al.,* 1987]. An example of the signature reversal is shown in Figure 3.9. In these L-band and X-band images collected in the East Greenland Sea during MIZEX '84 (an Office of Naval Research sponsored study of air-ice-ocean processes that take place at the marginal ice zone), the first year ice portions of the large multiyear floes produce stronger backscatter than the multiyear portions of the floe [*Cavalieri, et al.,* 1990]. In addition, the formation of pools of water open to the air or under thick layers of snow impacts the backscatter behavior of multiyear ice by creating regions of weak or strong returns dependent on radar wavelength. This scattering behavior is most prominent under peak melt. In addition, the magnitude of the signatures observed will be strongly dependent on frequency.

After peak melt, the melt pools may transition into thaw holes (vertical holes through the ice to the underlying water). A dried ice stage may follow where melt water has disappeared from the surface by draining through cracks or thaw holes in the ice. Rotten ice, a term applied only to first-year ice is next in the sequence. Here, the ice has become honeycombed and is in an advanced stage of disintegration. Flooded ice follows the rotten ice phase. At this point the ice is loaded with heavy wet snow and melt water. By mid-to-late summer, the backscatter from

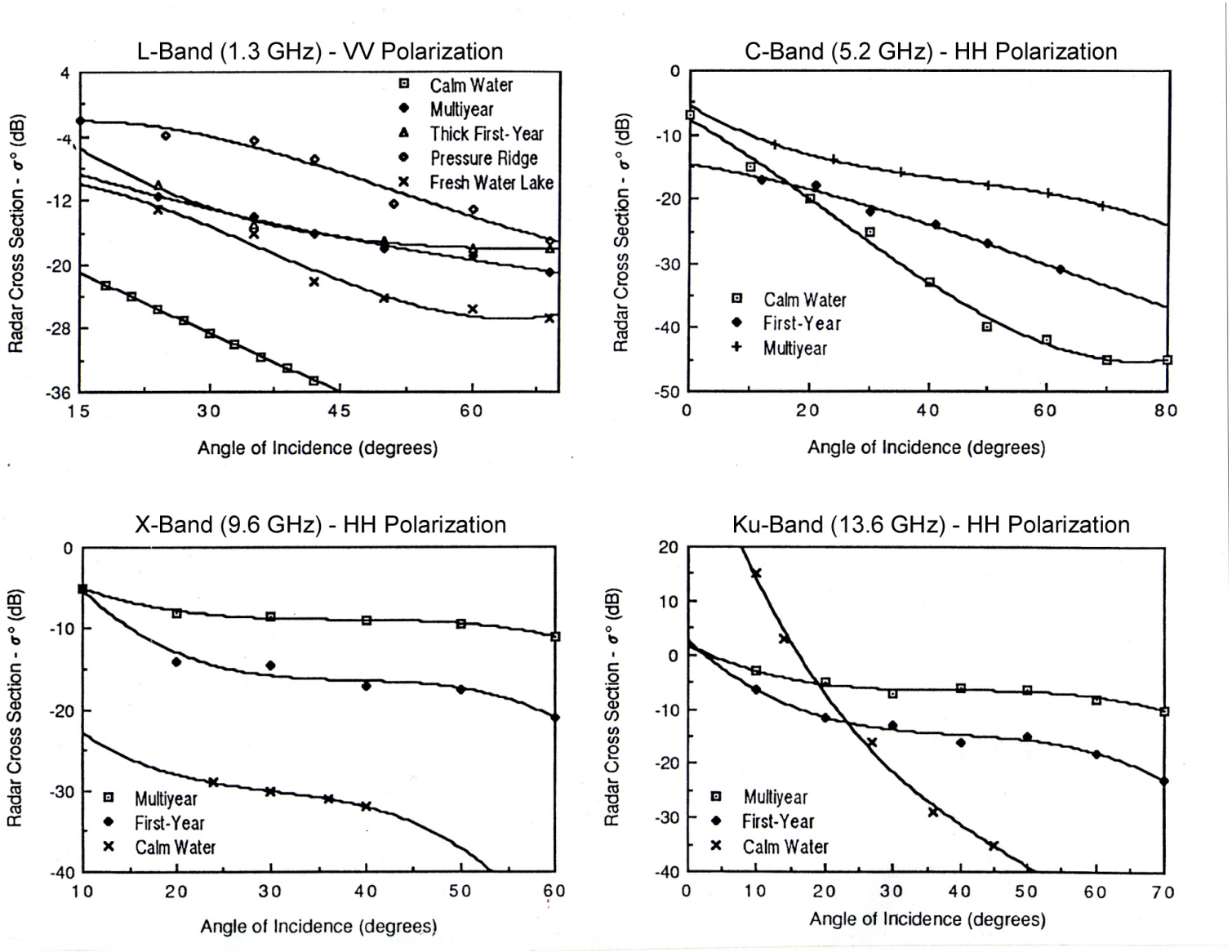

Figure 3.7. Radar backscatter cross-sections at L-, C-, X-, and Ku-bands during winter, illustrating the contrast in ice type and water signatures as a function of frequency and angle of incidence. [*Onstott*, 1992]

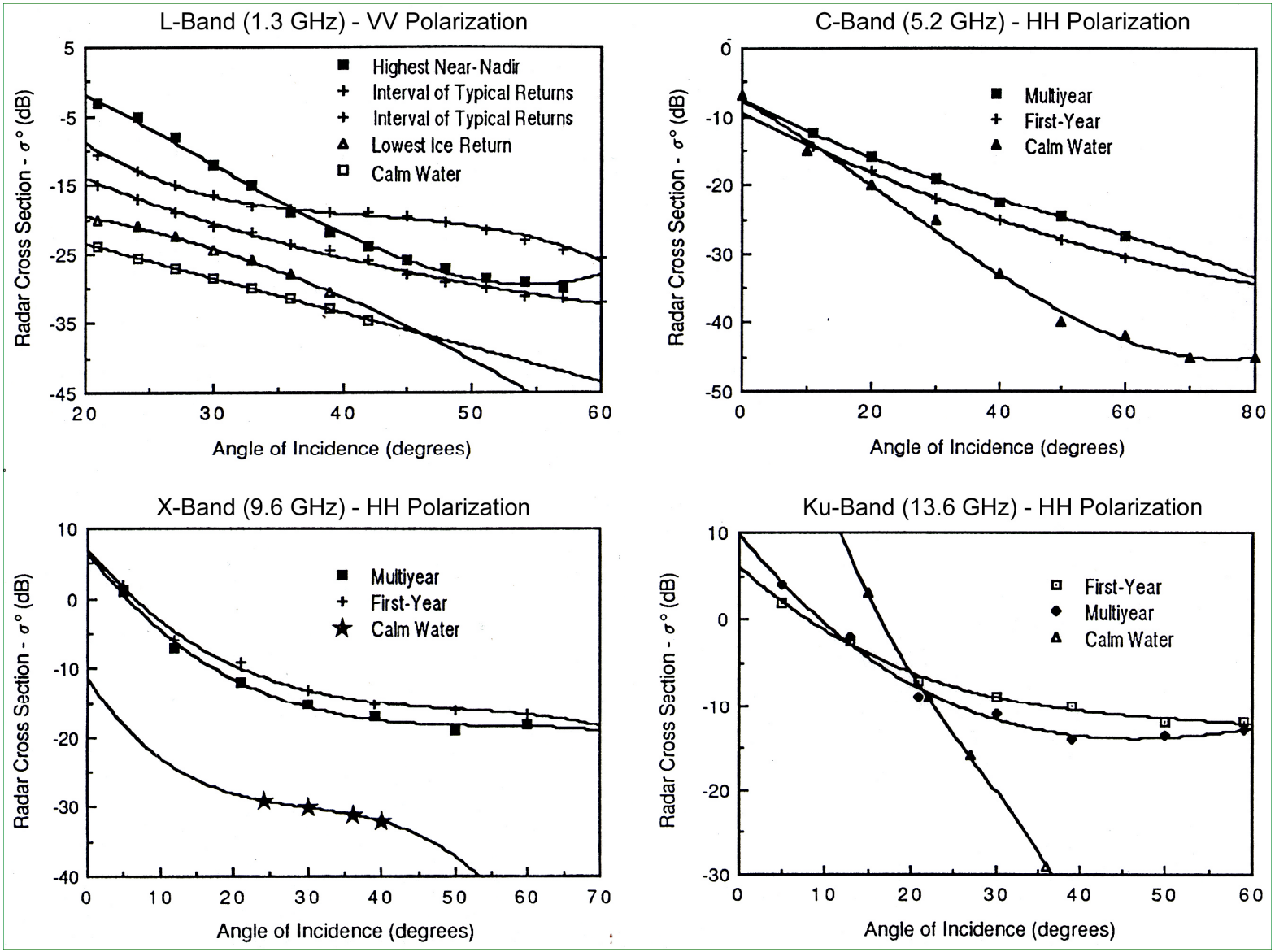

Figure 3.8. Radar backscatter cross sections at L-, C-, X-, and Ku-bands during summer, illustrating the contrast in ice type and water signatures as a function of frequency and angle of incidence. [*Onstott*, 1992]

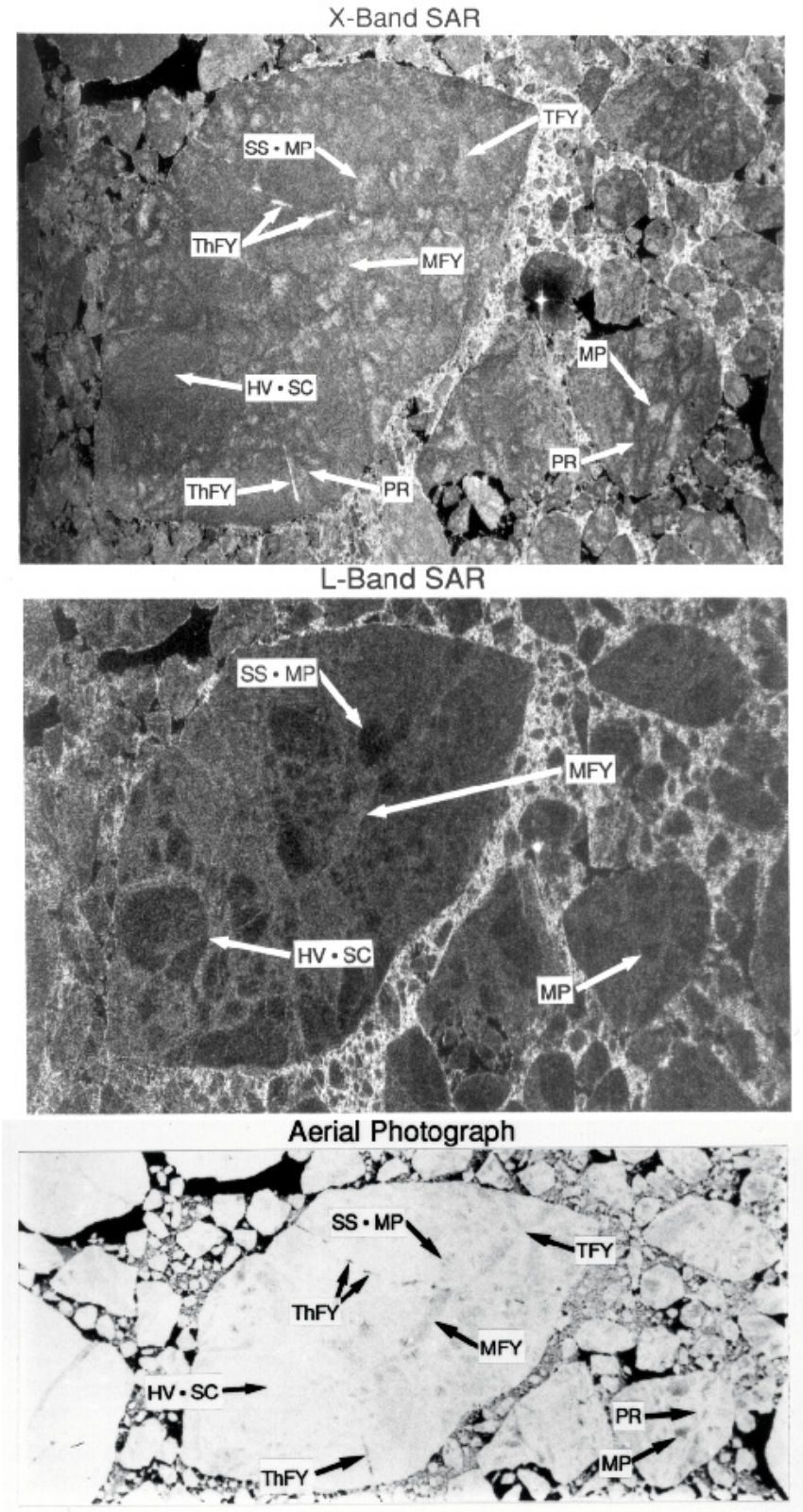

Figure 3.9. X- and L-band images of a large multiyear ice floe during the peak melt period during summer (29 June 1984). Notation: MFY - Medium FY, MP - Meltpool, PR – Pressure Ridge, HV SC - Heavy Snow Cover, ThFY – Thin FY, and SS – Saturated Snow [*Cavalieri et al.,* 1990] [*Onstott,* 1992].

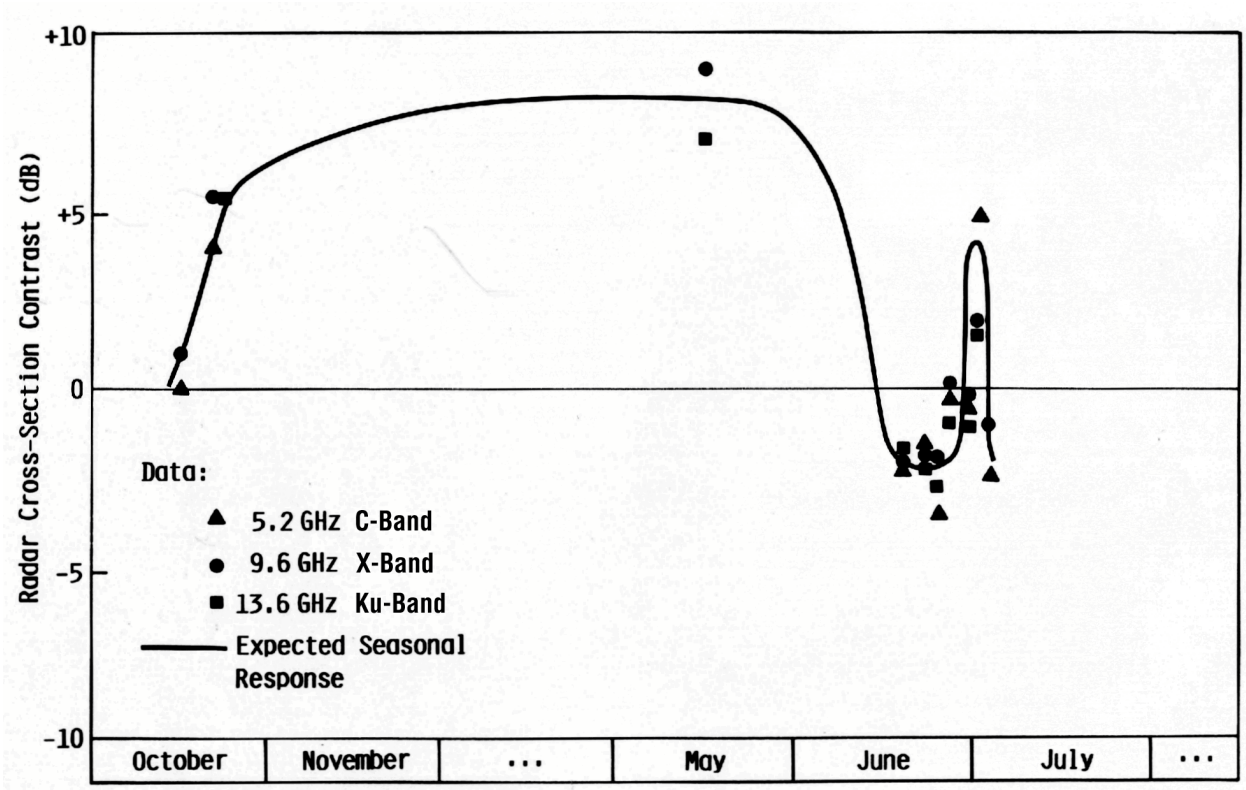

Figure 3.10. Contrast history illustrating contrast reversals that have been shown to occur between first-year and multiyear ice, the two major summer ice types for C-, X-, and Ku-band frequencies [*Onstott and Gogineni*, 1985].

multiyear ice becomes greater than that from first-year ice and the contrast between thin and thick ice increases with decreasing frequency (see Figure 3.10). This observation is explained by the fact that the multiyear ice is topographically rougher, has many tilted surfaces, and is a complex mixture of ice, snow, and water features that, in total, provide strong surface scatter. The roughness elements on the now snow-free, first-year ice are reduced in amplitude because of the continuation of melt. As surfaces become smoother, their backscatter intensities reduce.

3.4 Sea Ice in SAR Imagery

SAR imagery is being used to detect, locate, and identify a variety of sea ice forms and features that include: (1) ice type, (2) surface features, (3) floe size distributions and concentration, (4) ice edge, (5) leads and polynyas, (6) deformation, and (7) ice edge eddies and open ocean phenomena associated with the ice pack. Other features of interest may include: (a) icebergs and ice islands, (b) ships and platforms in the ice, (c) shore fast ice, and (d) waves in the pack ice.

3.4.1 Ice Type Determination

Sea ice type or thickness and age are extremely important parameters to measure and study in the polar oceans. Ice strength primarily depends upon ice thickness, age, salinity, and temperature. The distribution of ice thickness is important in climatic studies because it represents the outcome of the current growing season that is described by the duration and intensity of cold temperatures and ocean-atmosphere dynamics. Ice thickness is related to ice

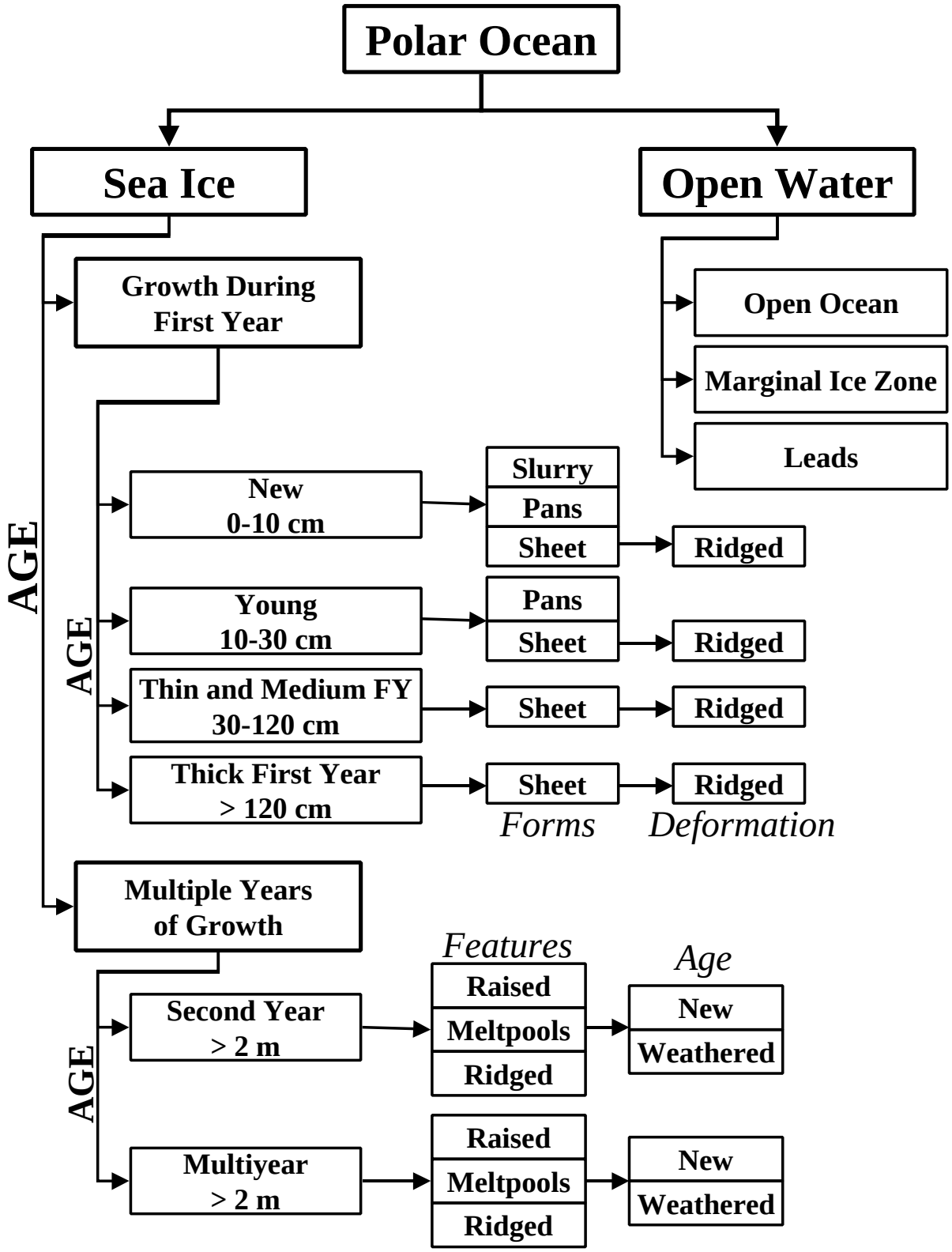

Figure 3.11. Topology of sea ice type, thickness, features and age.

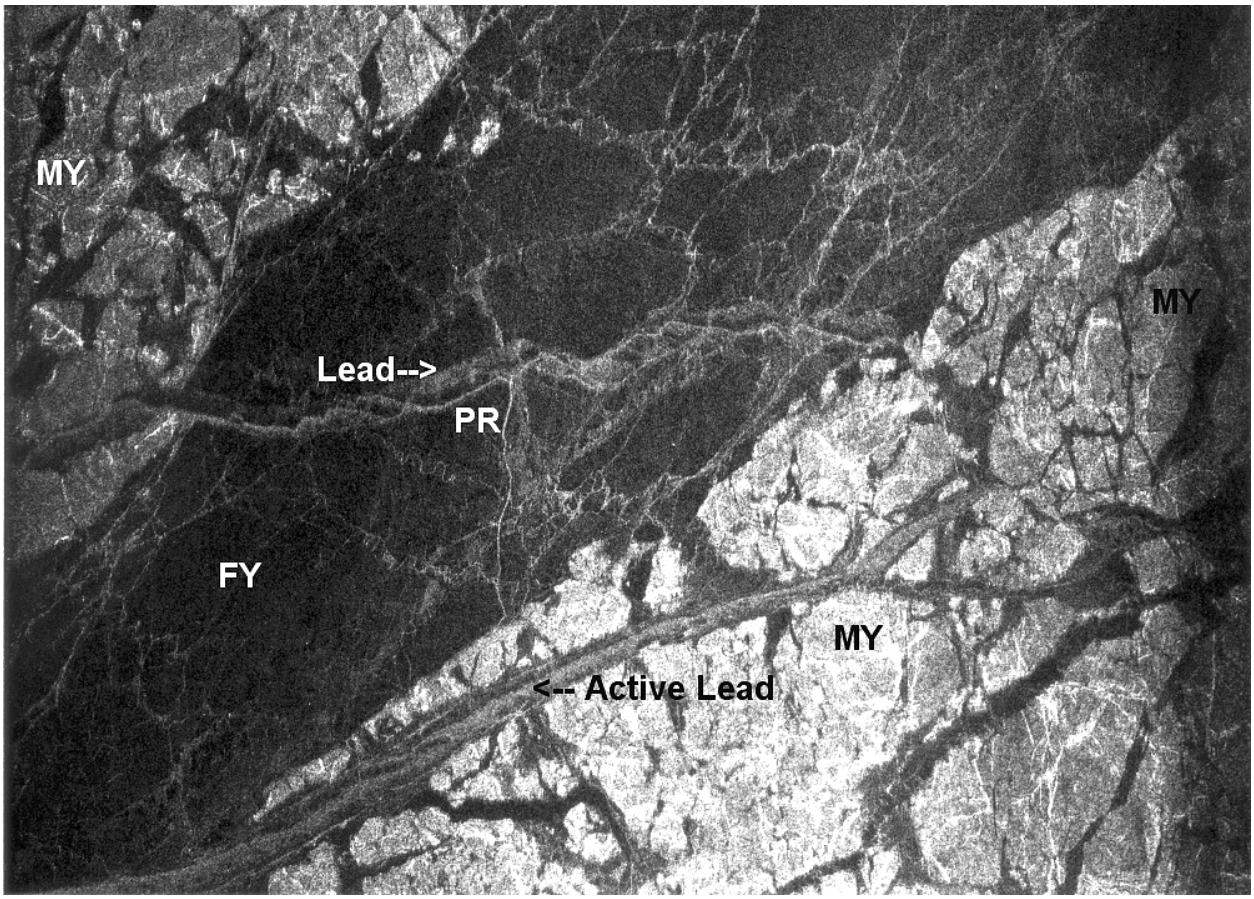

Figure 3.12. Winter C-band, VV polarization SAR pack ice example obtained from aircraft (incident angles from 20° to 70°) for the central Arctic during CEAREX'89. The imaged area is approximately 10 km wide.

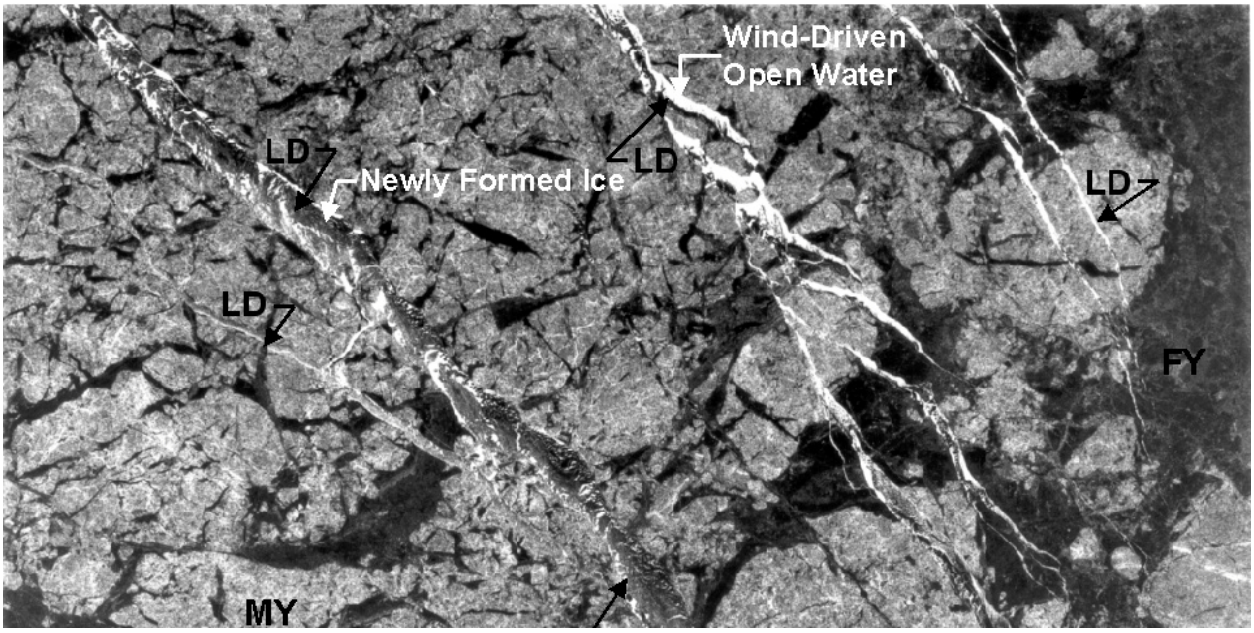

Figure 3.13. Winter ERS-1 (C-band, VV) SAR polarization image of pack ice with active leads (LD) in the Beaufort Sea from 24 March 1992. The imaged area is approximately 100 km wide. Original image © ESA 1992.

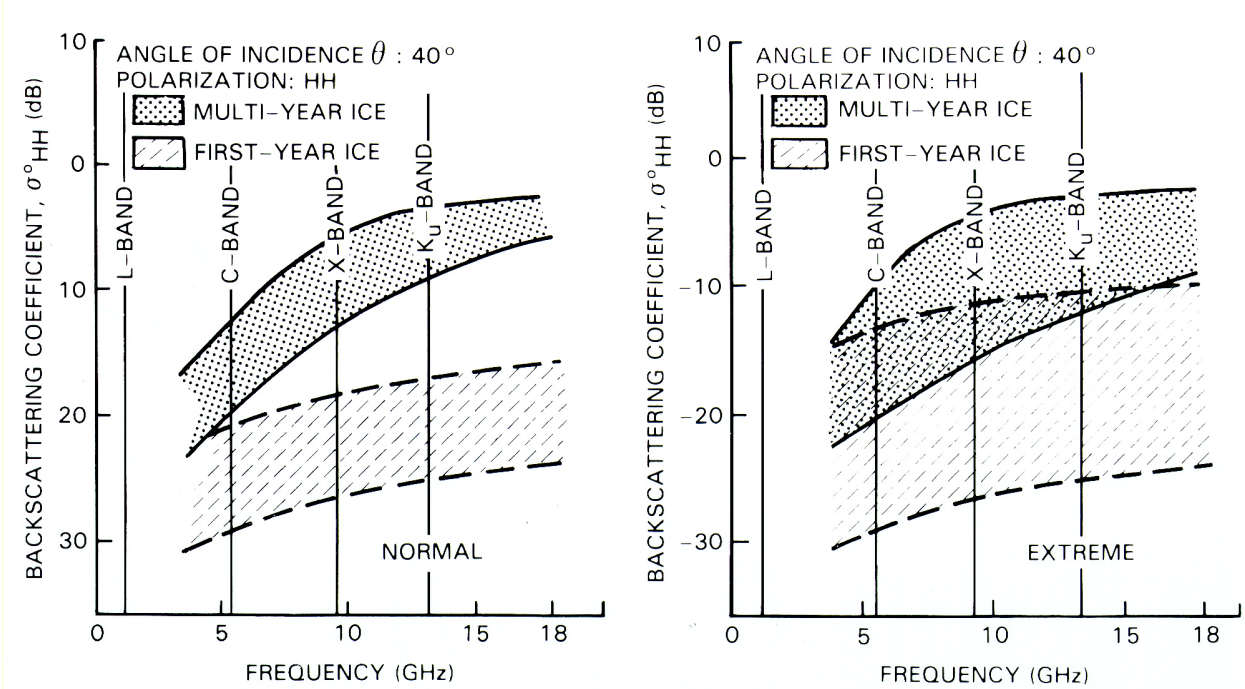

Figure 3.14. Frequency dependence of the backscatter coefficient for theoretical σ°s of multiyear and first-year ice under (a) normal/winter and (b) extreme/summer conditions is shown. [*Onstott*, 1992]

age, deformation caused by storms, and pressure in the ice pack. SAR imagery provides information on both age and thickness. This information is inferred from the backscatter intensity and how this intensity varies with position on the ice terrain surface. Figure 3.11 shows a topology of sea ice in order for the reader to associate ice age terminology with ice thickness, form, features, and deformation effects.

The dynamics during the freezing process have an impact on the physical structure of newly formed sea ice. If ice forms in an open lead when winds are calm, its surface may be relatively smooth. The effect of wind and waves is to produce ice with a rough surface with a higher dielectric constant. The backscatter response for recently formed ice is largely determined by the magnitude of its dielectric constant and surface roughness. The return from first-year, new ice, and open water is dominated by its surface roughness. Areas of first year ice that are exceptionally smooth, due to growth during very quiescent conditions, act as specular scatterers and produce very weak backscatter.

Multiyear ice with its lower salinity and greater ice penetration at microwave frequencies produces a backscatter response at C-band frequencies and higher which is dominated by volume scattering from the upper ice sheet gas bubbles and voids. Thus, the returns from multiyear ice are typically the brightest large area ice return in the imagery.

During winter, the microwave signatures of desalinated multiyear ice are clearly different from those of the saline first-year ice. This is very apparent in Figure 3.12 and 3.13. These C-band (VV) images were collected in the Beaufort Sea during winter. The multiyear floes are identifiable by their bright return and their floe shape; multiyear floes are typically more rounded than first year floes. In addition, note that the first year ice found in the pack ice appears as the backdrop in which multiyear floes are placed. This is also a good illustration of the way in which first year ice forms in the fall in this region and in the central Arctic. The radar signature

of multiyear ice is very stable during the period from about November through April in the Arctic. The first year ice framework that surrounds the multiyear ice is sufficiently weaker and discrimination between these two major ice types is not difficult. There are active leads found in both of the scenes.

In summary, the key discriminating features between first year and multiyear ice is (a) the difference in backscatter level, (b) that multiyear ice is found in well-defined and rounded floes, and (c) that multiyear ice has a very stable backscatter value during winter. Additional discussion of the evolution of first year ice is found in *Grenfell et al.* [1998] and *Perovich et al.*, [1998].

The active microwave backscatter of first-year and multiyear ice increases monotonically with increasing frequency and the radar contrast between these two ice types also improves with increasing frequency. Figure 3.14 shows the ability to discriminate first year ice from multiyear ice as a function of frequency at HH-polarization. Results for VV, HV, and HV are similar. Note the backscatter coefficient versus frequency plots confirm the assumption that higher SAR frequencies are better discriminators of ice type. The normal (winter) versus extreme (summer) illustrates the effect of liquid water in the snow cover during summer.

3.4.2 Ice Deformation and Surface Features

3.4.2.1 Ice Deformation. Wind and ocean forcing breaks ice into floes and, at the same time, deforms the ice by forcing it together or along the shore. Seasonal weather changes also affect the topography of the ice. Four types of processes control ice deformation: 1) fracturing, 2) hummocking, 3) ridging, and 4) weathering. Fracturing is a pressure process whereby ice is permanently deformed and rupture occurs. It is most commonly used to describe breaking across very close ice, compact ice, and consolidated ice. Hummocking is a pressure process that piles sea ice haphazardly one piece over another to form an uneven surface. When the floes rotate in the process, it is termed screwing. Ridging is a pressure process by which sea ice is forced upward into a line or wall called a ridge. The bright linear features running through both the first year (FY) and multiyear (MY) floes in Figure 3.12 are pressure ridges. Weathering is a process in which irregularities are gradually eliminated by thermal and mechanical means. Ice deformation can modify the backscatter signatures of both first year and multiyear ice.

3.4.2.2 Surface Features. Ice surface features are divided up into twelve categories according to the Ice Observation Handbook [1991]. The categories most commonly referred to are level ice, deformed ice, rafted ice, ridged ice, and hummocked ice.

Level ice is ice that has not been modified by deformation. Deformed ice is a general term for ice that has been squeezed together and, in places, forced upwards or downwards. Rafted ice is a type of deformed ice formed by one piece of ice overriding another; rafting occurs mostly on new and grey ice. A well-weathered ridge is a ridge that has experienced summer melt, has a sail that is rounded with slope of sides usually 20° to 30°, and is found on second and multiyear ice. A hummock may also be fresh or weathered with the submerged portion of broken ice under the hummock, forced downwards by pressure.

Figure 3.12 is a C-band (VV) SAR image from the Central Arctic collected during CEAREX [*Onstott and Shuchman*, 1990]. CEAREX was an Office of Naval Research study of ice in the Greenland Sea region that began during fall-freeze up (Year 1988) and continued monitoring ocean-ice-air processes well through winter (April 1989). Pressure ridges on the multiyear floes can also be observed on the image. Recently formed ridges (e.g., formed since

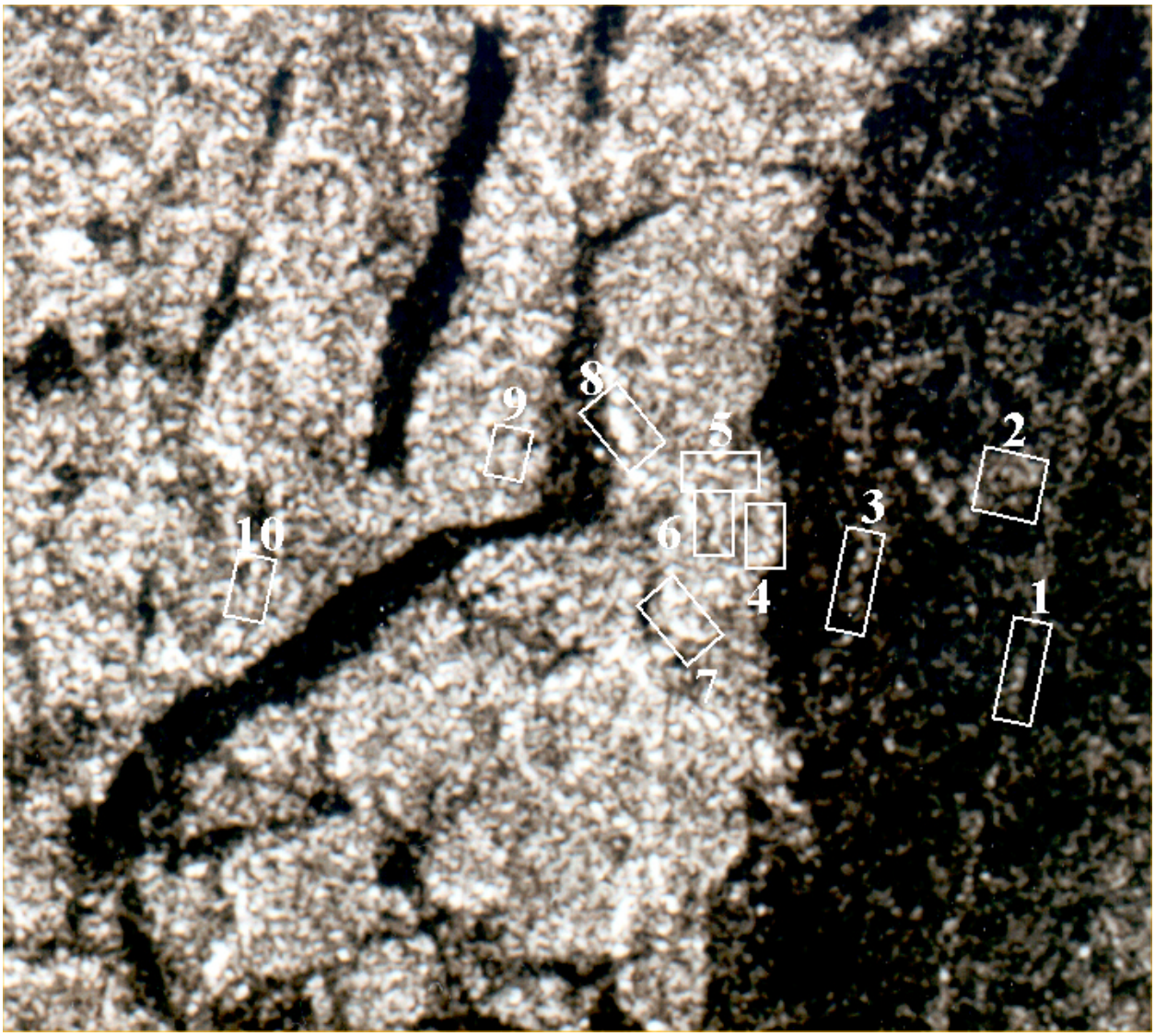

Figure 3.15. ERS-1 (C-band, VV) SAR image of multiyear and first year ice in the Beaufort Sea to illustrate pressure ridged ice responses. Annotated ridge information [ID#, Type, Height in Meters, Width in Meters]: [#1,FY,1-2.5,60-80], [#2,FY,2-4,34], [#3,FY,4.5,32-44], [#4, MY,5,34], [#5,MY,3.5,30], [#6,MY,5,28], [#7,MY,4-6,22-46], [#8,MY,-,24-33], [#9,MY,3-5,35-42], [#10,MY,3-4,25]. Radar viewed the scene from the left. The imaged area is 4.25 km wide. Original image ©ESA.

fall freeze-up) of multiyear year ice are observed as linear features that are brighter than the surrounding multiyear ice because structures of great vertical height with prominent height discontinuities produce strong returns. There are the occasional frozen melt pools that produce weak returns on a multiyear ice floe that can be observed at SAR ground resolution of 100 m. Surface features in the first year ice portions of the image include level ice (e.g., uniformly dark areas), pressure ridges (e.g., curvilinear bright features), extensive areas of deformed ice, and recently formed leads. At C- and X-band frequencies, recently formed leads will show regions of very weak to very bright return. Once a lead has aged a number of hours it will take on a uniform grey appearance with a backscatter intensity between that of FY and MY. Furthermore, for a few days its scattering coefficient may exceed that of MY ice if frost flowers form when the ice is young.

Ground surveys have been conducted to correlate pressure ridge characteristics with SAR backscatter intensity. Results show that the larger the mass of a ridge, the greater is its potential backscatter, and that the observed intensity is a maximum broadside to the ridge and minimum when viewing parallel to the ridge. Example ridge characteristics that include ridge height and ridge width are annotated on Figure 3.15 for illustration. Weathered multiyear ice ridges are topographically significant features associated with a multiyear floes, but are difficult to detect in SAR imagery because weathering greatly reduces vertical height discontinuities and rounds the ridge. These modifications work to reduce its backscatter intensity, making it more similar to that of level multiyear ice.

3.4.2.3 Leads and Polynyas. Leads and polynyas are important to ship operations, acoustic propagation, submarine surfacing, marine animal resource management, and climate change. A sea ice fracture is any break or rupture through compact ice, consolidated ice, fast ice, or single floe resulting from deformation processes. Fractures may contain brash ice and/or be covered with nilas or young ice and sizes may range from a meter to over 500 m.

A crack is a fracture that is only a few centimeters. A lead is any fracture or passageway through sea ice that is navigable by surface vessels. A polynya is any non-linear shaped persistent opening in ice. Examples of leads are shown in Figures 3.12 and 3.13. The image shown in Figure 3.13 was obtained in the Beaufort Sea within 50 miles from shore near Prudhoe Bay, Alaska. The leads shown are shore leads and form where the pack ice interacts with the landfast ice near the coastline. Lead activity in this region is dynamic and continuous.

Open water tends to freeze very quickly when the atmosphere is below –20°C and new ice will form and thicken quickly. Areas of first year ice that are exceptionally smooth, due to growth during very quiescent conditions, produce very weak backscatter.

Frost features form on new ice because of high humidity associated with an open lead. These features roughen the ice surface and act to raise the backscatter levels of young ice to values greater than those of smooth, medium, and thick first year ice. Within a few days, the frost feature effects dissipate and the young ice signature reduces to values approaching those of first year ice.

Frost features begin as fine ice crystal structures. Over periods of hours these features may cover a significant proportion of the ice surface and grow bases at the interface of the frost flower and the ice sheet comprised of granular ice. Some point in the formation process brine begins to wick from the ice sheet into the frost features known as frost flowers. With brine infiltration and surface roughening due to frost flower bases, the ice sheet's scattering coefficient experiences a dramatic increase. Frost flower sizes at the end of their life reach diameters as large as 5 cm and heights of 3 cm. Frost flowers survive a few days and are destroyed by wind and infiltration by snow crystals.

When wind conditions are high, such as greater than 7.5 ms^{-1}, the water surface remains clear of ice and ice crystals, and presents a backscatter response that is stronger than that of multiyear ice, if the radar incident angle is steep and the polarization is VV. This may not be the case for HH-polarization, or for large incident angles, as illustrated in Figure 3.13. Open water signatures in leads are typically associated with two wind regimes: high and calm. Strong winds are associated with storms that are robust enough to produce large leads. Otherwise, the winds tend to be calm and the leads tend to be small and well shadowed by the surrounding ice.

During February, March, and April of 1992, a lead was monitored to watch its evolution from birth through thirty-six days of life. A temporal sequence of images is presented in Figure

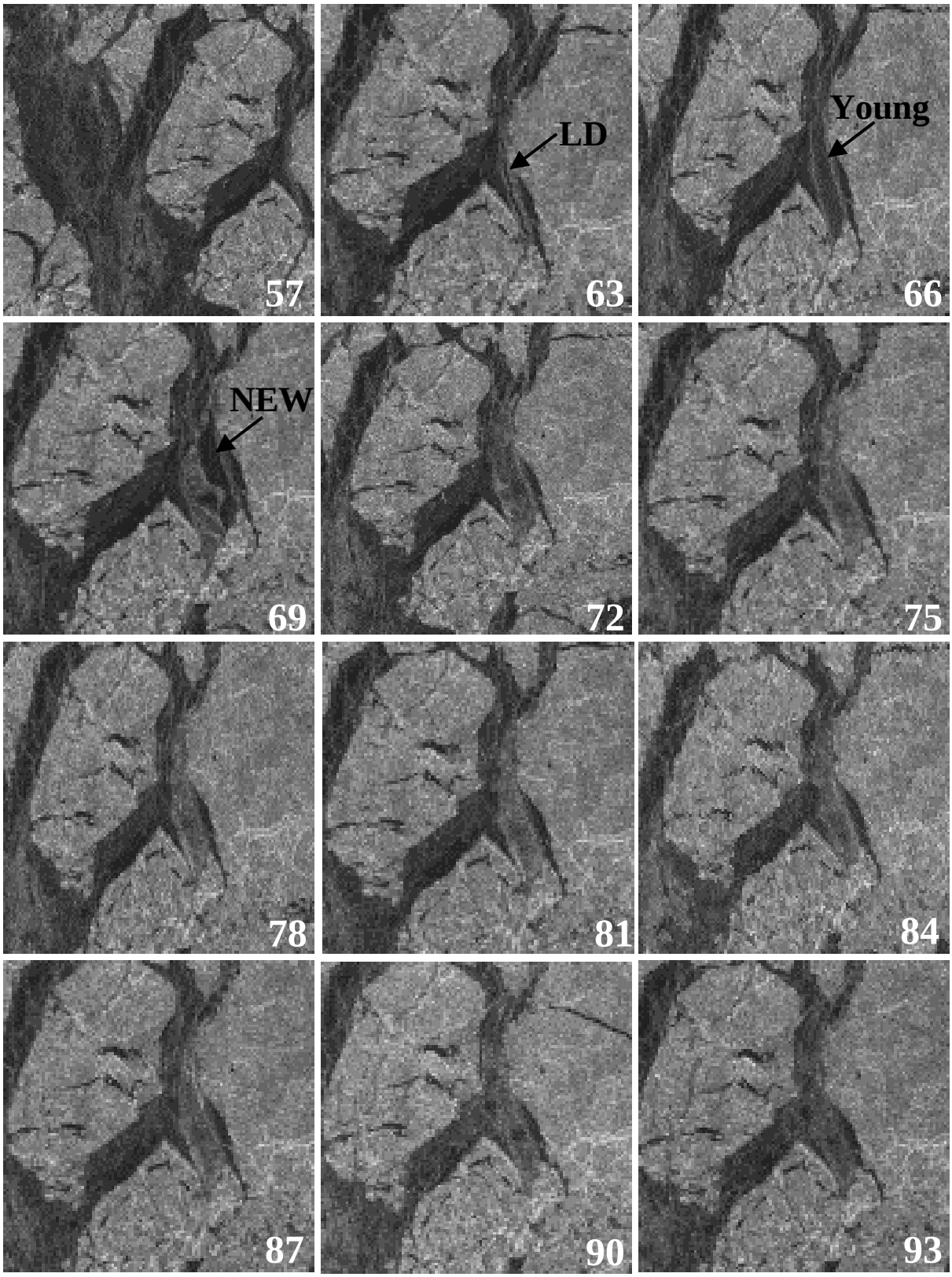

Figure 3.16. ERS-1 (C-band, VV) SAR imagery of a lead in the Beaufort Sea (about 72.5°N) during LEADEX'92 is shown as a function of day of year (DOY). Lead is located in center of image.

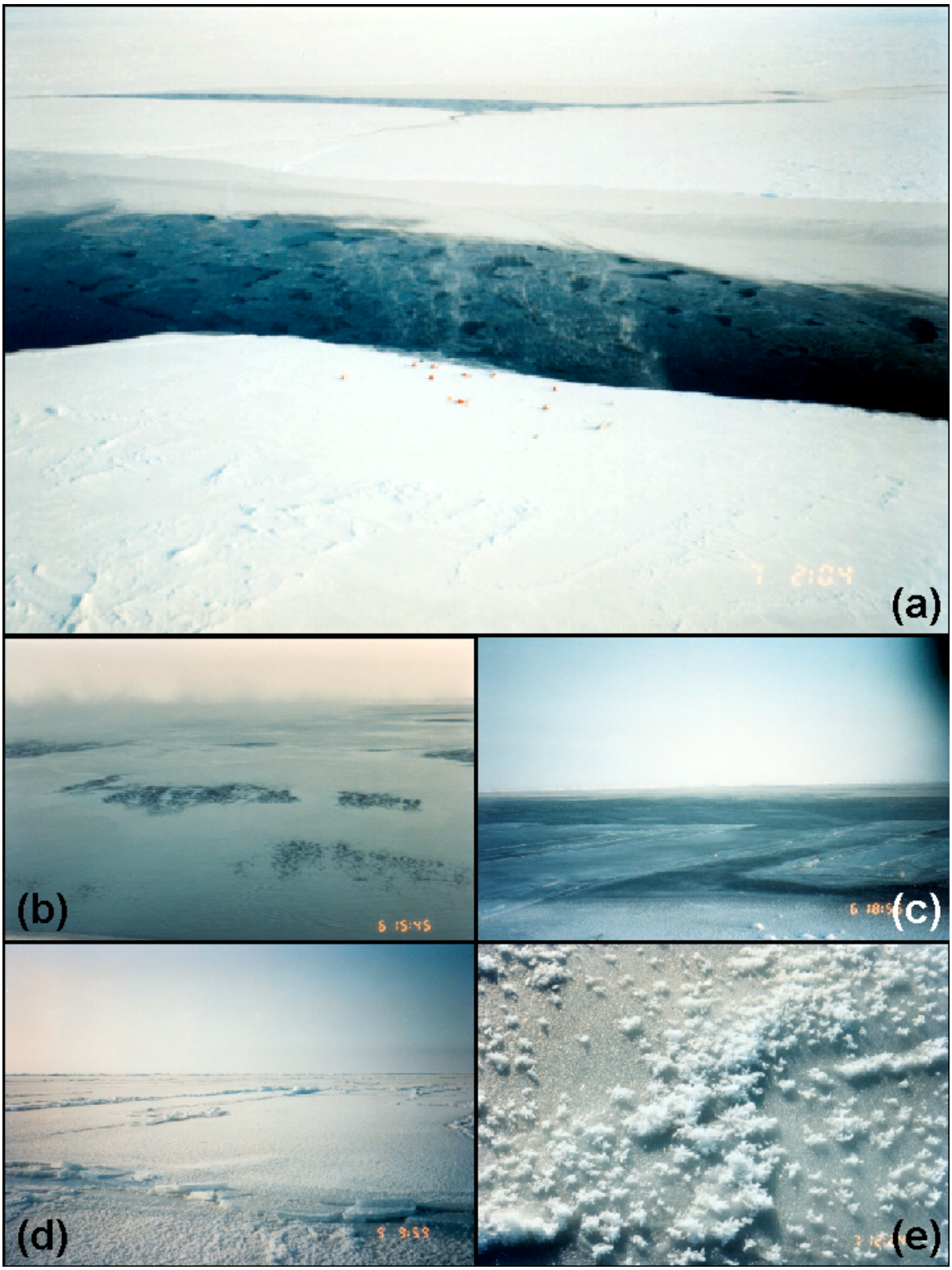

Figure 3.17. Photographs show the range of possible lead conditions in (a) a view of a large, recently opened lead, (b) the rapid formation of an ice skim and open water patches, (c) new ice formation with rafting, (d) aging to young ice with frost flowers, and (e) a close up of a frost flower.

3.16. The lead is located in the center of the images. As the lead ages, its shape and size change in response to forces in the ice pack. Ridge building events may pile lead ice on the surrounding first year ice (see DOY 66), highlighting the location of the lead with an enhanced backscatter level. When smooth new ice is produced, that portion of the lead signature is dark (see DOY 66). If frost flowers form (see DOY 75) or if ice becomes deformed, the lead signature brightens. With continued activity, the lead will present a variety of signature spatial responses (e.g., compare DOY 69 with DOY 93). As the lead ages the backscatter response level will begin to reduce as the frost flowers are destroyed and the ice desalinates (see DOY 93). As the ice thickens, it eventually becomes difficult to distinguish from the surrounding first year ice with a single frequency and polarization.

In Figure 3.17, a series of photographs document the ice conditions observed as a large lead evolved. A photograph taken from helicopter (see Figure 3.17a) shows the presence of a very thin ice layer and patches of open water with wind ripples (also see Figure 3.17b). After several hours a modest layer of new ice is present, but modified by rafting (see Figure 3.17c). Frost flowers formed and accompanied the visual whitening and backscatter enhancement of the lead ice (see Figure 3.17 d and e).

3.4.3 Determining Floe Size Distributions and Concentration

3.4.3.1 Floe Size. The high-resolution capability of SAR makes it the ideal sensor to observe ice floe size boundaries and concentration [Burns et al., 1987]. Sea ice does not necessarily form as a solid sheet of ice. The effects of wind, swell, currents, tides, and thermodynamics contribute to ice formation and break-up. The resulting pieces all have various names according to their size (see Table 3.1, from the Ice Observation Handbook).

Sea ice concentration is typically expressed in tenths of area coverage. For example, 9 tenths is 90 percent ice cover. Ten-percent concentration or less is considered open water. Ice concentration is highly variable with the greatest water concentration found at the very end of the melt season, and the lowest water concentration at the end of the growing season.

Example images obtained during the summer in the Greenland Sea are shown in Figure 3.9 and are typical of the summer ice field conditions. The figure shows X-band and L-Band SAR images, in addition to an aerial photograph, and was taken nearly coincidentally from aircraft. First, note that the aerial photograph shows excellent contrast between ice and water. The SAR imagery also shows a high contrast level since the water produces weak backscatter due to floe shadowing of the wind which produces lead water with a smooth surface, while the ice response is greater because of surface scattering. In addition, brash ice (e.g., small ice pieces) and small floes between the larger floes have rough ice-air interfaces and produce strong backscatter at all satellite frequencies and also act to highlight floe boundaries. The floe that dominates these images is a vast multiyear ice floe that is bonded together with thin zones of first year ice of different ages. Surrounding this ice floe are small to large multiyear ice floes. It is also important to note that during summer the thin ice regions within the multiyear floe have enhanced backscatter response at X-band because of a lack of snow cover and roughened ice surfaces.

The floe field may move by wind or currents. Shearing may occur and divergence-convergence zones may result. In the divergence zones, the ice sheets part and open water is exposed to the atmosphere. Open water will freeze very quickly when the atmosphere is below -20°C unless winds keep the water agitated.

Table 3.1. Floe Size Descriptors [Ice Observation Handbook, 1991]

Name	Abbreviation	Dimensions
Brash	BSH	< 2m
Pancake	PH	30 cm – 3 m
Ice Cake	CK	20 m or less
Small Floe	SF	20-100 m
Medium Floe	MF	100-500 m
Big Floe	BF	500 m – 10 km
Vast Floe	VF	2 km – 10 km
Giant Floe	GF	> 10 km

3.4.3.2 Concentration. At present, the primary tool to determine global ice concentration and multiyear ice fraction is the Special Sensor Microwave Imager (SSM/I). SAR may also be used, and is especially useful when finer ice concentration detail is required. Figure 3.18 is an illustration of the ice concentration and multiyear fraction derived using X-band SAR (aircraft) for the MIZ in March 1989. The color bar shows ice concentration values from 0 to 100%. Concentrations vary from 100% in the ice interior to about 50% in the MIZ. The multiyear ice fraction is spatially variable and ranges from about 20% to 90%. Advanced Very High Resolution Radiometer (AVHRR) visible and thermal images are shown for comparison (see Figure 3.17b). A composite product is shown in Figure 3.17c and includes SSM/I concentrations for large area coverage. Superimposed on the SSM/I data is SAR-derived concentration for added detail in a portion of the pack and MIZ regions, ice surface temperature contours derived using AVHRR, and SSM/I derived near surface winds.

3.4.4 Ice Edge Characteristics and Detection

The ice edge is the demarcation at any given time between the open water and sea ice of any kind. It may be a regular line with compacted floes, it may consist of a succession of belts or strips, or it may be frayed with off-lying isolated fragments or pancake ice. The ice edge is highly variable and exhibits rapid dynamic and thermodynamic responses. If the wind direction changes, the ice edge responds. This may mean a dramatic change in position, and going from a compact to a diffuse edge within a day to two. If ambient conditions cool sufficiently and certain circumstances occur, large expanses of newly formed ice may suddenly appear. A discussion of processes found at the ice in the Arctic is presented in Chapter 18. Detailed discussion of pancake ice, which is an important contributor to the ice signature of the marginal ice zone, is found in *Onstott et al.* [1998].

Variations in ice concentrations along the edge result from wind drag, tides, ocean circulation, ice ablation, or freezing and can vary on a daily, monthly, seasonal, or yearly basis. Ice edges are either compacted or diffuse. Compacted edges are clearly defined due to wind and/or currents. They are typically on the upwind side of the pack. Diffuse edges are poorly defined and are usually associated with the downwind side of the pack.

The type of ice edge can be identified by observing the change in the ice concentration within the outer ice edge region that is made up of pans, cakes, and small, broken-up floes. These small floes will range from 20 to 100 m in diameter and form because of ablation, freezing, and gravity wave/ice interaction, and eddy induced collisions that break up large floes.

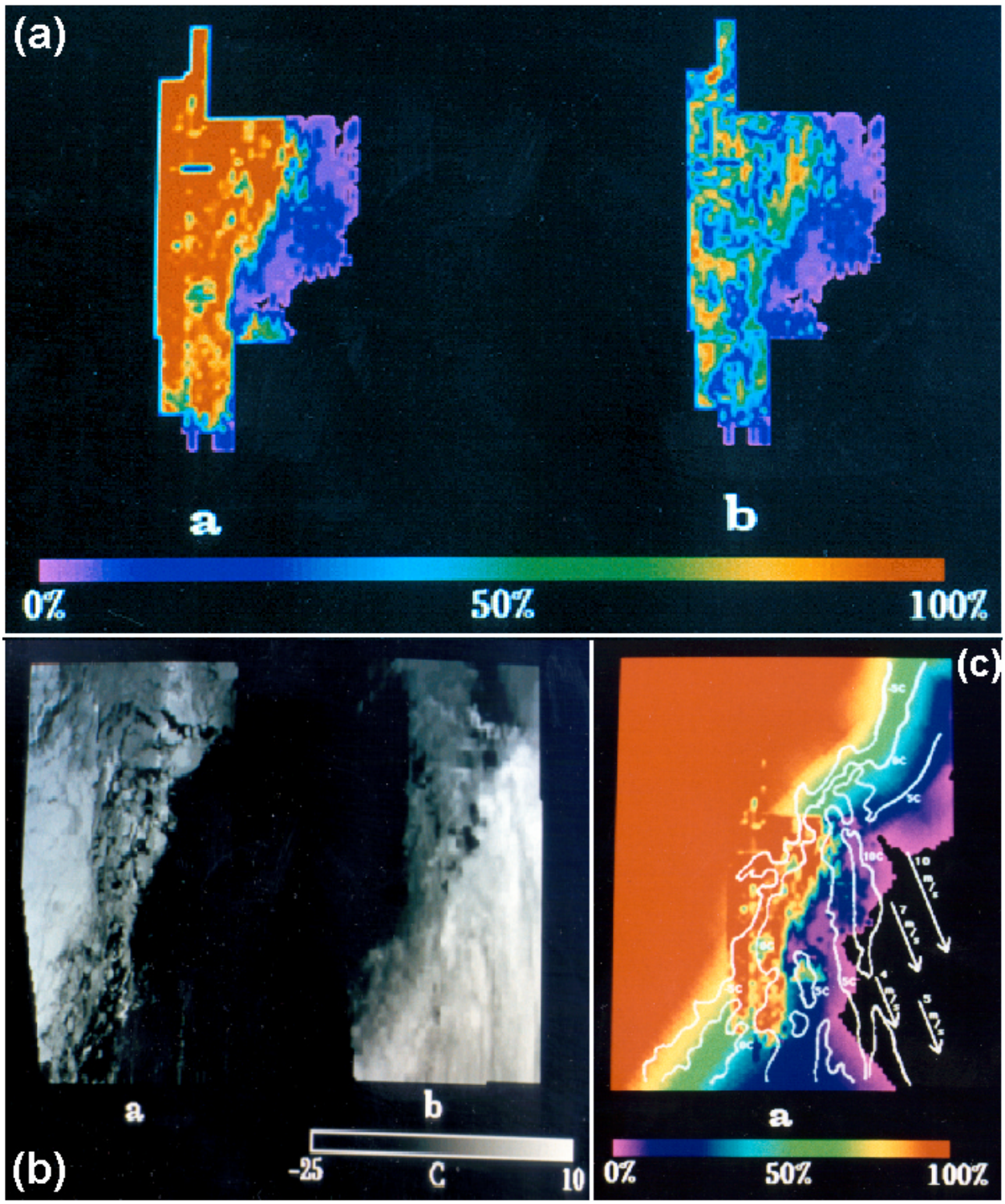

Figure 3.18. Ice concentration (a-a) and multiyear ice fraction (a-b) derived from SAR, and AVHRR visible (b-a) and AVHRR-IR (b-b) are shown for the marginal ice zone in the Greenland Sea for 20 March 1989. SSMI ice concentration is the basis for (c). The SAR-derived ice concentration, surface temperature, and ocean wind speeds are also shown in (c).

When an on-ice wind event occurs (e.g., when the wind blows toward the ice), the ice edge will then be compact. During these events, locating the edge on SAR imagery is quite easy. When winds blow from the pack ice to the open water, a diffuse edge forms and the zone is composed of both ice and open water, and can be spread over a very wide area making delineation of an open water and ice boundary very difficult.

Two examples of ice edge conditions found in the Arctic are shown in Figures 3.19 and 3.20. Figure 3.19 is an X-band (HH) mosaic collected by aircraft on 31 March 1987 during MIZEX'87 at incident angles from 50° to 75°. Concentrated ice composed of cakes and small floes is compacted along the outermost regions to form a distinct ice/open water boundary. Light to moderate wind speeds of 5 to 10 m s^{-1} were recorded for the day. During the winter season, the C- and X-band SAR data can be used to differentiate between ice types. Bright tones on the image represent multiyear ice, while darker tones are various stages of first-year and young ice. The darkest signatures are open water because of the middle to large incident angles used. Note an ice tongue (T) and numerous bights (B) are visible on the image. An ice tongue is a projection of the ice edge several kilometers in length, caused by wind or current. A bight is an extensive crescent shaped indentation in the ice edge, formed by either wind or current. In the upper right hand portion of the image are ice patches or small ice fields well away from the compacted ice edge and into the open ocean. An ice field is an area of drift ice consisting of floes of any size and having an area greater than 10-km across. An ice patch is simply an area of drift ice less than 10-km across.

The ice edge location is determined by some combination of ocean circulation, bathymetry, tides, wind direction and speed, and ice ablation or freezing. The seaward migration of the ice edge resulting in a diffuse or unclear delineation between ice and open water is the result of either meandering ocean currents or an off-ice wind and is ultimately controlled by ice ablation.

Wind is a determining factor in discerning the ice edge in SAR imagery. High wind and wave conditions particularly when imaged at small (less than 35°) incident angles will cause the open (ice free) ocean to give a large return making the intensity value similar to sea ice. However, an experienced analyst can still differentiate between the two. The wind for the image shown in Figure 3.19 was 10 m s^{-1} from the north.

In Figure 3.20 is an example of a diffuse ice edge. This is an L-band, HH-polarization image collected using SEASAT. The open ocean typically produces a moderate to strong response. A very thin layer of ice crystals or frazil has formed at the ice edge and the small capillary wind waves are dampened and a weak backscatter response results. Pancake ice and small ice floes are typically present at the outermost positions of the edge and present a return as bright or brighter than the open ocean due to the rough ice surface and water-ice boundary scattering.

3.4.5 Snow on Sea Ice

Snow on ice plays a variety of roles that affect the ability of SAR to characterize sea ice. In winter, the dry snow pack and upper portion of the ice sheet are at temperatures much less than 0°C. The surface of multiyear ice under the dry snow can be flat, mounded, or depressed (e.g., filled with frozen melt water). Each surface is characterized by a different backscatter value. On cold multiyear ice, snow with depths greater than 2 m has been shown to be essentially transparent at frequencies below 10 GHz; however, on very smooth first-year ice, snow may dominate the microwave signature [*Kim, et al.,* 1985]. Furthermore, if the snow

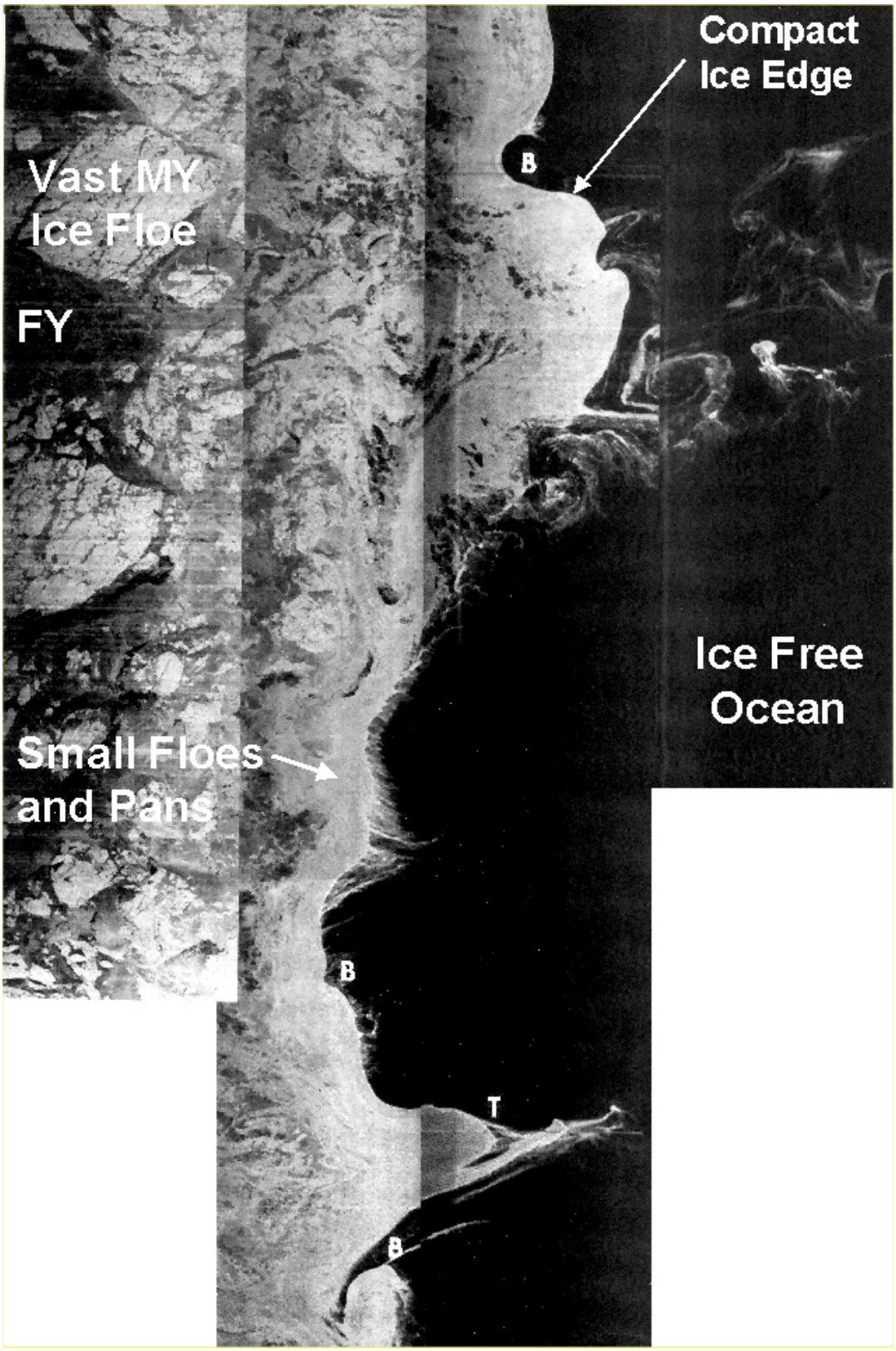

Figure 3.19. X-band (HH) mosaic obtained by aircraft of the marginal ice zone in the Greenland Sea (about 78.5° N and 3° W) during 31 March 1987. The imaged area is approximately 60 km wide.

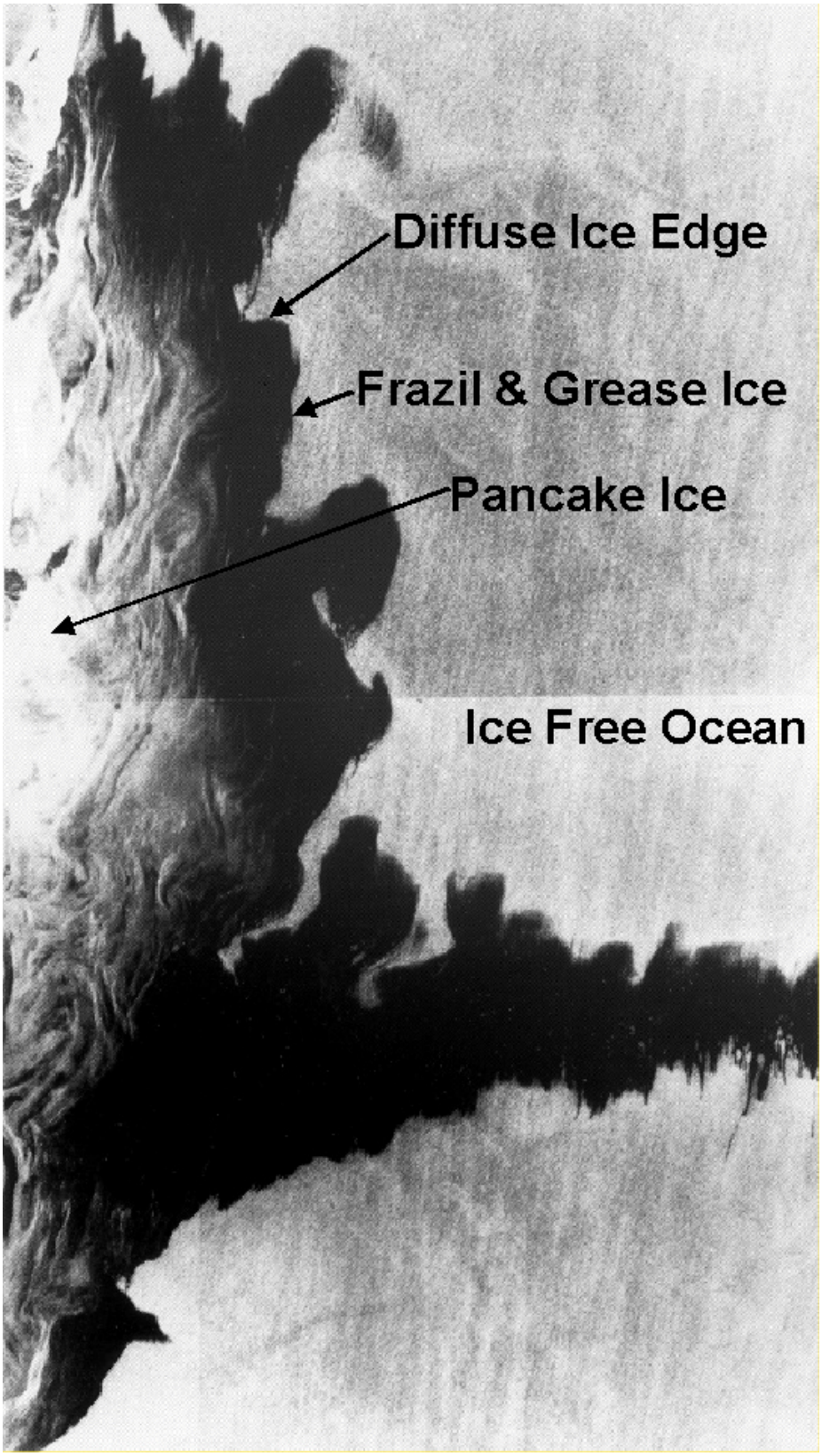

Figure 3.20. SEASAT (L-band, HH) image of Chukchi Sea during October 1978. The imaged area is approximately 200 km x 100 km.

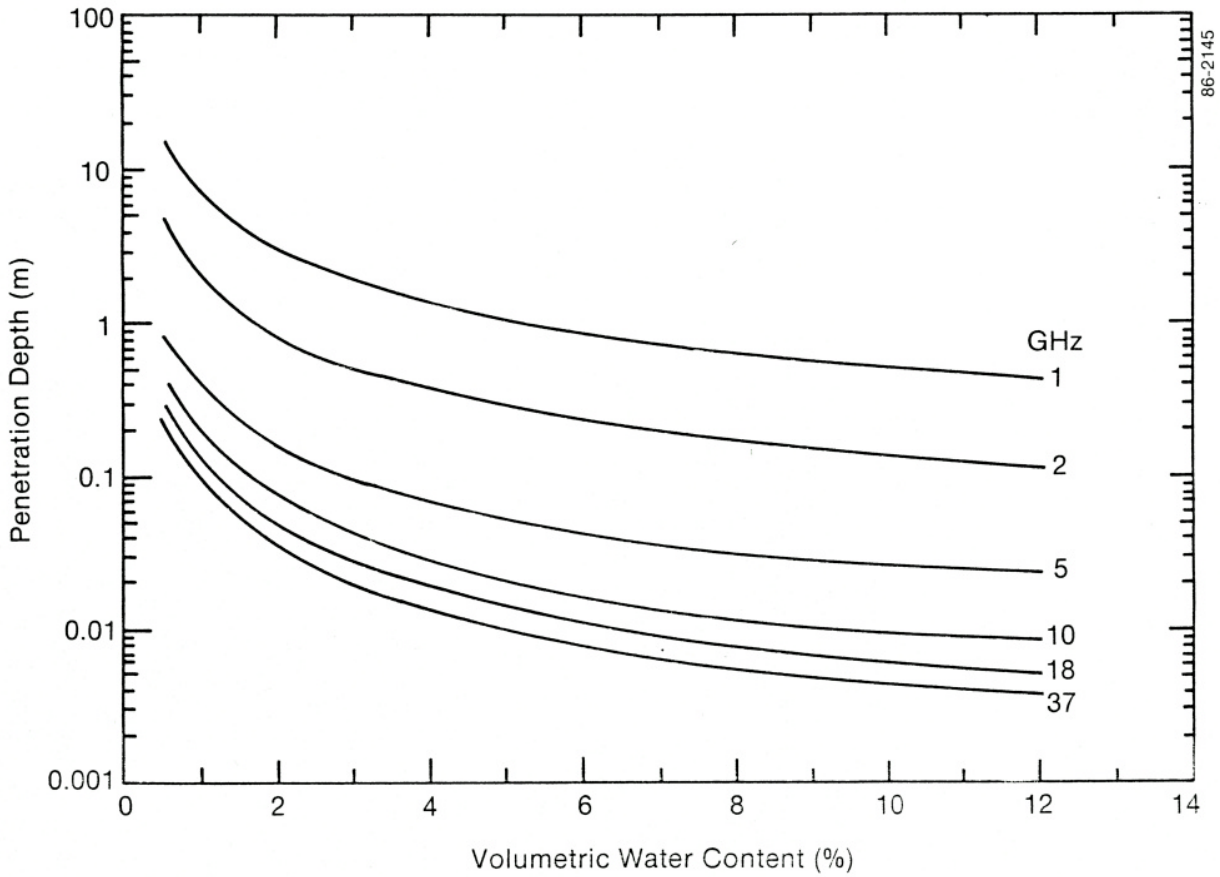

Figure 3.21. Penetration depth for snow with a density of 385 kg cm^{-3} for frequencies between 1 and 37 GHz - calculations are based on experimental data acquired and results published by *Matzler* [1985], *Hallikainan et al.*, [1984], and *Tiuri et al.*, [1984].

thickness becomes too large, the ice sheet is pushed below sea level, floods with seawater, and attains a first-year ice signature, independent of the previous ice form.

Arctic lows may also pass through a region during the spring, and the upper portion of the snowpack may experience melt and refreeze. The snow crystals may enlarge and a multiyear-like signature may be produced if the radar wavelengths are 1 cm or smaller. At current SAR operating frequencies, this snow crystal effect is negligible. In addition, moisture from the humid snow layer may collect on the cold ice surface and freeze. This superimposed ice roughens the ice-snow interface. The roughness of this layer increases during the early stage of the melt process and eventually becomes the key contributor to the backscatter signatures of thin to medium first-year ice.

During early summer, the snow layer has a more dominant role. This is illustrated by the critical relationship between frequency, the volumetric liquid water content in the snow and penetration depth (Figure 3.21). The penetration depth is dramatically reduced with even a fraction of a percent of liquid water (a quantity so small that present direct measurement methods provide this value only with great difficulty). The penetration depth is further reduced with increasing wetness or increasing frequency. For example, in the Fram Strait region during the summers of 1983 and 1984, the bulk wetness of the snowpack was found to stay at about 5 or 6% [*Onstott, et al.,* 1987]. The penetration depth at a 30-cm wavelength (L-Band) (note that $\lambda = c/f$,

where c is the speed of light and f is frequency) is about 1 m, but at a 6-cm wavelength (C-band), it is only about 5 cm. Snow thickness prior to melt was about 45 cm on thick ice.

As summer progresses, the major role of the snowpack is to produce free water, which moistens the snow and accumulates into pools. Typically, there are alternating mounds and pools of ice and water. By midsummer, the snow pack has experienced considerable melt. Accumulations of meltwater on multiyear ice and thick first-year ice create slush layers, sometimes many centimeters thick, and drainage of water into depressions contributes to the formation of subsurface melt pools. An important change in the summer microwave signature occurs when the snow becomes completely saturated with water, creating slush. At this point, the backscatter signature is increased beyond that of moist snow because of accompanying increases in surface roughness and dielectric constant.

After midsummer, open water melt pools become common on thick ice where about 50-60% of the snow has melted. A snow-ice crust may be in place on elevated multiyear ice surfaces, on thick first-year ice, and on multiyear ice. On thin first-year ice and medium first-year ice, the snow pack may have eroded into a 2-cm-thick granular snow-ice layer, and former melt pools may consist of collections of candied ice tips that rise about 1 cm above the freeboard of the thin, saturated ice sheet.

3.4.5.1 Sea Ice Backscatter Modeling. Attempts have been made to explain theoretically the backscatter from sea ice. Models, when successful, prove useful in interpreting the microwave signatures of the many ice forms. Results have been used to refine and focus the measurement of physical and electrical properties in sea ice investigations. One of the first attempts to model the backscatter behavior of sea ice was conducted by *Parashar et al.* [1978]. An important leap forward in the modeling of multiyear ice was made by *Fung and Eom* [1982] by combining volume scattering with a rough surface model. A parametric study by *Kim et al.* [1984] allowed an examination of the sensitivity of the microwave signature to changes in key ice sheet parameters, including salinity, temperature, brine volume, density, air bubble size, and surface roughness. The effect of snow on sea ice was then described in *Kim et al.* [1985]. Additional modeling studies of data collected in the field and during laboratory measurements are summarized in *Winebrenner et al.* [1992], *Barber et al.* [1998], and *Golden et al.* [1998a, 1998b]. Most recent modeling efforts have been directed at understanding the coherence properties of electromagnetic scattering [*Nghiem et al.*, 1995].

3.4.6 Polarization and Sea Ice

Future satellite SARs will have the capability to operate at four transmit-receive polarization combinations coherently (e.g., VV, VH, HV, and HH). This type of radar is referred to as fully polarimetric. Future satellite SARs that have this capability and that will provide coverage in the Polar Regions are named PALSAR (Japanese, L-band) and RADARSAT-2 (Canadian, C-band).). ENVISAT, (European, C-band), currently has the capability to collect all four polarimetric combinations but not simultaneously.

Polarization describes the orientation of the electric field vector of the electromagnetic wave as it propagates. It is an important factor when distinguishing between various ice types and form. Vertically polarized waves may interact with a surface geometry in different ways than horizontally polarized waves, resulting in a different radar backscatter between the two.

A SAR image set showing frequency and polarization behavior of Beaufort Sea Ice is presented in Figure 3.22. These data were obtained using the JPL AIRSAR. Shown in the figure

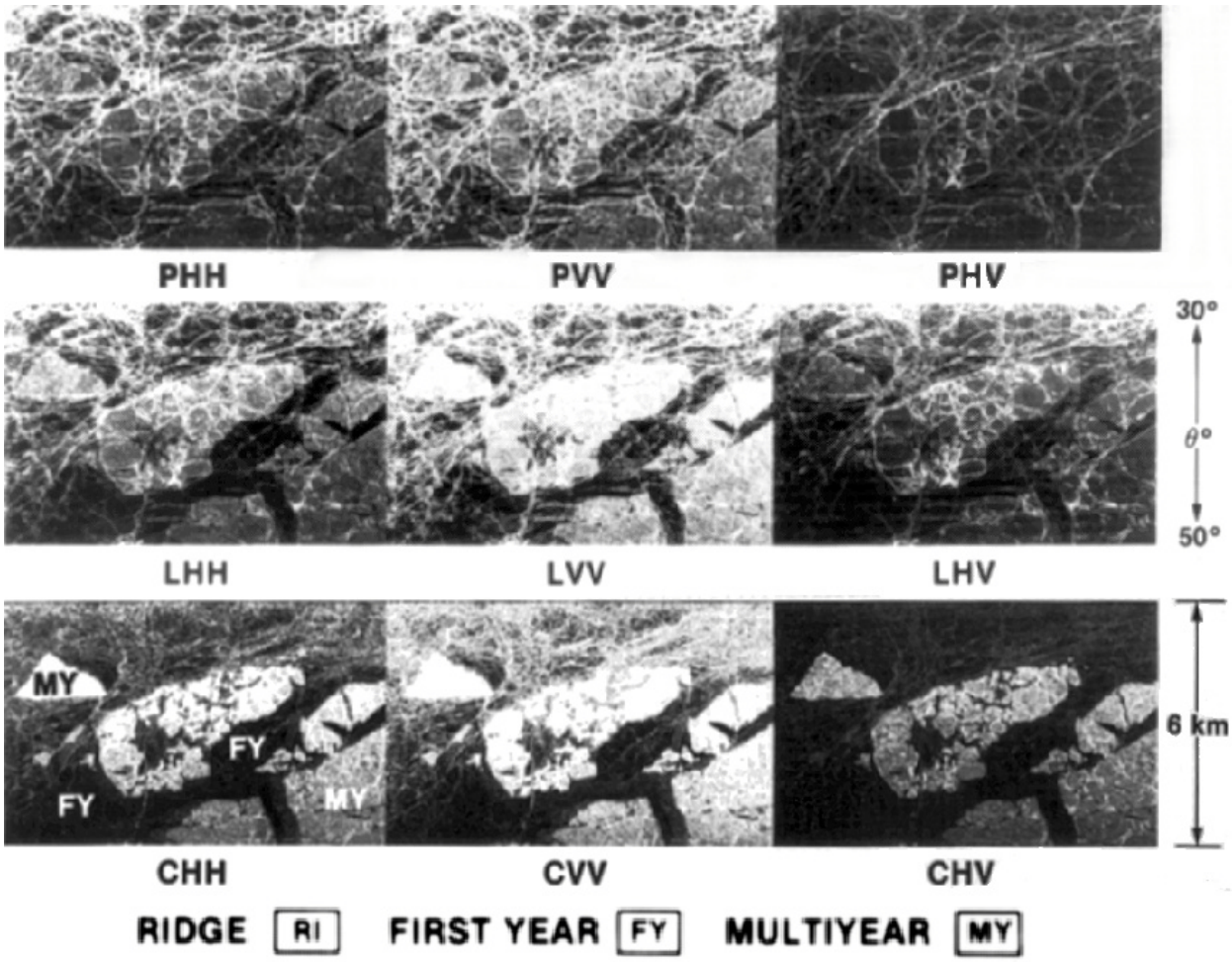

Figure 3.22. JPL AIRSAR image (listed by band and polarization) of polarimetric Beaufort Sea Ice data.

are images acquired at P-band (60 cm), L-band (25 cm), and C-band (5 cm) and with VV-, HH- and VH-polarization. The two primary ice types present are first year and multiyear (annotated in the C-band image). Primary ice forms include level and deformed ice.

An interesting factor of note with this image set is that the wavelength change from the highest to lowest frequency is a factor of twelve. Over a wavelength change this large, it would be expected that the ice property information presented in the SAR image data would be different. In addition, with the addition of polarization information, it would also be expected that additional ice information would be obtained. Results to date suggest that both of these expectations are true, and that additional information will be gained by using multifrequency and polarimetric radars. As new satellite capability comes online, how to exploit additional frequency, polarization, and incident angle information will continue to be of great interest.

It is known that longer wavelengths penetrate further into sea ice. In addition, the degree of the surface roughness that is required to produce strong backscatter scales with wavelength. Hence, long SAR wavelengths will require large surface height variations to produce strong backscatter. In examining the P-band images in Figure 3.22 it is apparent that it is difficult to make out the multiyear floe structure. In addition, the prominent image features are thin and curvilinear. This makes it clear that a P-band radar is most sensitive to surface topography, such as pressure ridges. It could not be determined if fractures in the ice floes contributed to the

backscatter response. There is a weak sense of ice type differences. It appears that the delineation of the multiyear floe boundaries in a first year ice matrix is marginally possible. VV-polarization is best for floe boundary detection. The HV-polarization is best if a map of surface topography is desired since all ice type information is suppressed.

The information content at L-band images falls in between that of P- and C-band. The surface topography of the ice floes dominates the information content, but there is added ice type information over that provided at P-band. The presence of multiyear ice is more easily detected, and floe boundary delineation is improving. Again VV-polarization is best at providing ice type and floe boundary information. Cross-polarization provides the best surface topography information, but in a more confused fashion than that at P-band (e.g., limited to the largest topographical features).

The discrimination of first year from multiyear ice is most easily accomplished using C-band data. This discrimination is easily made at each of the three polarizations. The optimum polarization for this discrimination, however, has now changed to either HH or HV. The deformed first year ice portion of the VV data reduces its effectiveness. Multiyear ice detection is most easy in the cross-polarization channel because the small- and large-scale surface roughness effects are greatly reduced.

SEASAT and JERS-1 SARs operated at L-band which was determined to not be particularly good for differentiating ice types. Conversely, the ERS-1, ERS-2, and RADARSAT-1 SARs operated at C-band, were found to work quite well for differentiating among major ice types during winter.

Multiyear ice and first-year ice can be distinguished in the winter independent of wavelength within the C to Ku portion of the microwave region. However, in the spring and summer, discriminating first-year from multiyear ice becomes difficult because of the free water in the snow, and on the ice surfaces, and warm upper ice volume. The free water prevents significant microwave penetration, eliminating the volume scattering that distinguishes the multiyear ice return.

One example of how polarization sensitivity may be exploited is in the discrimination between open water and ice. There is a significant difference between the electrical properties of open water and ice (about an order of magnitude). Because of this difference and the polarization sensitivity of backscatter from a rough surface, a comparison of the ratios of backscatter for two orthogonal polarization sets (i.e., vertical-transmit and vertical-receive with horizontal-transmit and horizontal-receive) for these two ice forms results in an exploitable difference. Furthermore, with the discrimination of open water, new ice may then be discriminated by detecting weak return areas within lead regions. This capability was demonstrated using aircraft SAR imagery, and represents a key opportunity for future space-based polarimetric radar.

Additional examples of polarization behavior of sea ice and its application to the classification of sea ice may be found in *Drinkwater et al.* [1992].

3.4.6.1 Polarimetric Discriminants. The term polarimetric discriminants utilized here is defined in terms of the elements of the covariance matrix. The polarimetric discriminants include phase difference, span, depolarization ratio, and correlation coefficient.

Phase Difference

One of the pieces of new information provided by a polarimetric radar is phase difference. It is the result of the examination of the correlation of the two co-polarization

returns, specifically the difference between the phase at HH and VV polarizations. This information may be retrieved from the covariance matrix by performing the calculation where

$$q_{VVHH} = \tan^{-1}\left|\frac{(\mathrm{Im} < S_{HH}S_{VV}^{*} >)}{(\mathrm{Re} < S_{HH}S_{VV}^{*} >)}\right| \tag{4}$$

A simple manmade target made of a conducting material will produce a mean phase difference of 0° and a probability distribution that is very narrow, if not a delta function. Complex shapes and multiple reflections have been observed which often produce non-zero phase difference values. The phase differences for plane dielectric surfaces are known to increase with increasing angle. Phase differences may originate from polarization sensitivity to the population of scatterers in the clutter scene where scatterer Set A dominates HH backscatter, while a scatterer Set B dominates VV backscatter. Large local slopes also contribute to differences. For natural clutter mean phase differences are typically near 0°. Distribution width is often related to complexity of the composition of the clutter scene that includes local slope, element size, and dielectric property distributions.

Total Power or Span

Span is the term used to represent the total power of the scatter field. It may be calculated accordingly

$$SPAN = < S_{HH}S_{HH}^{*} > + < S_{VH}S_{VH}^{*} > + < S_{HV}S_{HV}^{*} > + < S_{VV}S_{VV}^{*} > \tag{5}$$

Depolarization Ratio

The depolarization ratio has been defined here as the ratio of the power associated with the copolarization elements of the scattering matrix and the cross polarization elements. It is defined as

$$Pd = \frac{< S_{HH}S_{HH}^{*} > + < S_{VV}S_{VV}^{*} >}{< S_{VH}S_{VH}^{*} > + < S_{HV}S_{HV}^{*} >} \tag{6}$$

One of the advantages of this definition for depolarization ratio is that it allows for an intuitive understanding and provides a reduction in the variance since it is composed of four elements rather than just two.

Correlation Coefficient

The correlation between the copolarization elements (VV and HH) is defined

$$r_{HHVV} = \left|\frac{< S_{HH}S_{VV}^{*} >}{\sqrt{< S_{HH}S_{HH}^{*} >< S_{VV}S_{VV}^{*} >}}\right| \tag{7}$$

Expected Utility of Polarimetric Discriminants

The expected utility of the polarimetric discriminants is presented in Table 3.2.

Table 3.2. Expected Utility of Polarimetric Discriminants

Discriminant	Utility
Phase Difference	Difference in the phase of the like polarizations. Its value is determined by the magnitude of the ice or water dielectric constant. The largest difference will be observed for new ice, the smallest for MY ice. Phase difference assists in separating open water from ice.
Total Power or Span	Provides feature fill in, improves feature delineation, and reduces signal variance.
Depolarization Ratio	Aid in discriminating ice type and determining ice age. MY ice will have a high ratio. New ice will have the lowest ratio. FY ice will fall in between.
Correlation Coefficient	Utility is yet to be determined.
Polarization Ratio	Ratio of the like polarizations. Its value is determined by the magnitude of the ice dielectric constant. The largest ratio will be observed for open water and new ice. MY and FY ice have ratios near 1. This ratio will assist in separating open water from ice.

3.5 Summary

This chapter presented the fundamentals of active microwave remote sensing of sea ice. Empirical data, collected over a wide range of frequencies, polarizations, and angles of incidence, have contributed to the use of microwaves to classify ice type and to characterize the physical and electrical properties that control emission and backscatter levels. The other ice chapters in the Manual show how by understanding the processes and properties responsible for producing microwave signatures from sea ice, it has been possible to develop approaches to retrieve critical geophysical parameters including: edge characteristics, type, floe size distribution and concentration, thickness, age, and snow cover.

3.6 References

Barber, D. G., A. K. Fung, T. C. Grenfell, S. V. Nghiem, R. G. Onstott, V. Lytle, D.K. Perovich, and A. J. Gow., 1998: The role of snow on microwave emission and scattering over first-year sea ice. *IEEE Trans. Geosci. Remote Sens.*, **36**, 1750–1763.

Carsey, F. D., Ed., 1992: *Microwave Remote Sensing of Sea Ice*. *Geophys. Monogr.*, No. 68, Amer. Geophys. Union, 462 pp.

Cavalieri, D. J., B. B. Burns, and R. G. Onstott, 1990: Investigation of the effects of summer melt on the calculation of sea ice concentration using active and passive microwave data. *J. Geophys. Res.*, **95** (C4), 5359–5369.

Drinkwater, M. R., R. Kwok, E. Rignot, H. Israelsson, R. G. Onstott, and D. P. Winebrenner, 1992: Potential application of polarimetry to the classification of sea ice. F. D. Carsey, Ed., *Microwave Remote Sensing of Sea Ice*, *Geophys. Monogr.*, No. 68, Amer. Geophys. Union, 419–430.

Fung, A. K., and H. J. Eom, 1982: Application of a combined rough surface volume scattering theory of sea ice and snow. *IEEE Trans. Geosci. Remote Sens.*, **20**, 528–536.

Golden, K. M., and Coauthors, 1998a: Inverse electromagnetic scattering models for sea ice. *IEEE Trans. Geosci. Remote Sens.*, **36**, 1675–1704.

——, and Coauthors, 1998b: Forward electromagnetic scattering models for sea ice. *IEEE Trans. Geosci. Remote Sens*., **36**, 1655–1674.

Grenfell, T. C., and Coauthors, 1998: Evolution of electromagnetic-signatures of sea ice from initial formation through the establishment of thick first-year ice. *IEEE Trans. Geosci. Remote Sens*., **36**, 1642–1654.

Hallikainen, M., F. T. Ulaby, and M. Abdeirazik, 1984: The dielectric behavior of snow in the 3 to 37 GHz range. *Proc. IGARSS'84 Symp.*, Paris, France, European Space Agency, 169–174.

Haykin, S., E. Q. Lewis, R. K. Raney, and J. R. Rossiter, 1994: *Remote Sensing of Sea Ice and Icebergs*. Wiley and Sons, 686 pp.

Ice Observation Handbook, 1991: Prepared by: Commanding Officer, Naval Polar Oceanography Center, 4301 Suitland Rd Washington, DC 20395-5180, 118 pp.

Kim, Y. S., R. K. Moore, and R. G. Onstott, 1984:Theoretical and experimental study of radar backscatter from sea ice. University of Kansas Report #RSL TR 331-37, Lawrence, Kansas, 168 pp.

——, R. G. Onstott, and R. K. Moore, 1985: The effect of a snow cover on microwave backscatter from sea ice. *IEEE J. Oceanic Eng*., **9**, 383–388.

Matzler, C., 1985: Interaction of microwaves with natural snow cover. lnstitute of Applied Physics, University of Bern, Habilitationsschrift 152, Bern, Switzerland, 148 pp.

Nghiem, S. V., R. Kwok, S. H. Yueh, and M. R. Drinkwater, 1995: Polarimetric signatures of sea ice: 1. Theoretical model. *J. Geophys. Res*., 100 (C7), 13 665–13 679.

Onstott, R. G., 1980: Radar backscatter study of sea ice. Ph.D. thesis, University of Kansas, 250 pp.

——, 1992: SAR and Scatterometer Signatures of Sea Ice. F. D. Carsey, Ed., *Microwave Remote Sensing of Sea Ice, Geophys. Monogr.*, No. 68, Amer. Geophys. Union,, 73 – 104.

——, and R. A. Shuchman, 1990: Comparison of SAR and scatterometer data collected during CEAREX. *Proc. IGARSS'90 Symp*., College Park, MD, IEEE, 1513–1516.

——, and S. Gogineni, 1985: Active microwave measurements of Arctic sea ice under summer conditions. *J. Geophys. Res.*, **90**, 5035–5044.

——, R. K. Moore, and W. F. Weeks, 1979: Surface-based scatterometer results of Arctic sea ice. *IEEE Trans. Geosci. Electron*., **17**, 78–85.

——, ——, S. Gogineni, and C. Delker, 1982: Four years of low altitude sea ice broadband backscatter measurements. *IEEE J. Oceanic Eng*., **7**, 44–50.

——, T. C. Grenfell, C. Matzler, C. A. Luther, and E. A. Svendsen, 1987: Evolution of microwave sea ice signatures during early and mid summer in the marginal ice zone. *J. Geophys. Res.*, **92**, 6825–6835.

——, P. Gogineni, A. J. Gow, T. C. Grenfell, K. C. Jezek, D. K. Perovich, and C. T. Swift, 1998: Electromagnetic and physical properties of sea ice formed in the presence of wave action. *IEEE Trans. Geosci. Remote Sens*., **36**, 1764–1783.

Parashar, S. K., A. K. Fung, and R. K. Moore, 1978: A theory of wave scatter from an inhomogeneous medium with a slightly rough boundary and its application to sea ice. *Remote Sens. Environ*., **7**, 35–50.

Perovich, D. K., and Coauthors, 1998: Field observations of the electromagnetic properties of first-year sea ice. *IEEE Trans. Geosci. Remote Sens*., **36**. 1705–1715.

Smith, Walker 0., Jr., Ed., 1990: Remote Sensing of the Polar Oceans. *Polar Oceanography, Part A: Physical Science*, Academic Press, 123–170.

Tiuri, M., A. Sihvola, E. Nyfors, and M. Hallikainen, 1984: The complex dielectric constant of snow at microwave frequencies. *IEEE J. Oceanic Eng*., **9**, 377–382.

Vant, M. R., R. B. Gray, R. O. Ramseler, and V. Makios, 1974: Dielectric properties of fresh sea ice at 10 and 35 GHz. *J. Appl. Phys*., **45**, 4712–4717.

——, R. O. Ramseier and V. Makios, 1978: The complex dielectric constant of sea ice at frequencies in the range 0.1 - 40 GHz. *J. Appl. Phys.*, **49**, 1264–1280.

Winebrenner, D. P., 1992: Microwave sea ice signature modeling. F. D. Carsey, Ed., *Microwave Remote Sensing of Sea Ice, Geophys. Monogr.*, No. 68, Amer. Geophys. Union, 137–176.